Marine and Petroleum Geology 94 (2018) 144–165

Contents lists available at ScienceDirect

Marine and Petroleum Geology

journal homepage: www.elsevier.com/locate/marpetgeo

Research paper

Geometric and depositional responses of carbonate build-ups to Miocene sea level and regional tectonics offshore northwest Australia

James Van Tuyl*, Tiago M. Alves, Lesley Cherns

3D Seismic Lab, School of Earth and Ocean Sciences, Cardiff University, Main Building, Park Place, CF10 3AT, Cardiff, United Kingdom

ARTICLE INFO

Keywords:
North west Australia
Browse basin
Miocene
Carbonate reefs
Carbonate facies
Seismic attributes
Outcrop analogue
Reservoirs

ABSTRACT

The geometric and depositional responses of isolated carbonate build-ups to Miocene sea-level change and regional tectonics are investigated using 3D seismic and borehole data from the Browse Basin, North West Australia, combined with outcrop information from the Cariatiz Reef, southeast Spain. The interpreted seismic volume documents five (5) Miocene sequence boundaries and five (5) main seismic facies. Seismic attribute analyses proved to be a highly effective tool for interpreting carbonate facies but, when compared with outcrop information from southeast Spain, attribute data are limited to features larger than 16.4 m vertically, and 18.75 m horizontally. Estimations of reservoir potential are thus significantly underestimated when only based on the interpretation of seismic data. As a corollary of the structural analysis in this work, growth patterns suggest Messinian structural partitioning across the Browse Basin, with deformation associated with plate collision focused on preferentially oriented faults, i.e. only influencing carbonate build-up evolution at a local scale.

1. Introduction

Carbonate-hosted reservoirs are significant hydrocarbon exploration targets (Saqab and Bourget, 2015), and are estimated to comprise half of the world's hydrocarbon reserves (Ahr, 2008). The production of hydrocarbons from such a type of reservoirs is particularly important in equatorial regions of the Middle East (Harris and Frost, 1984; Ehrenberg et al., 2007), Indonesia (Kusumastuti et al., 2002), or the Philippines (Neuhaus et al., 2004), to provide a few examples. In addition to their economic importance, carbonate sequences often record the tectonic and sedimentary evolutions of continental margins (Chang et al., 2017). Carbonate build-up evolution and geometry, in particular, are influenced by a combination of tectonic processes such as faulting and accelerated subsidence (Saqab and Bourget, 2015; Rosleff-Soerensen et al., 2012, 2016; Zampetti et al., 2004), as well as sea-level change, oceanographic processes, geostrophic currents and local sedimentary processes (Mutti and Hallock, 2003; Anselmetti et al., 2000; Kenter, 1990).

Located offshore Northwest Australia, the Browse Basin is one of a series of sedimentary basins developed on the so-called North West Shelf (Stephenson and Cadman, 1994; Rosleff-Soerensen et al., 2012, 2016) (Fig. 1). Carbonate deposition in the Browse Basin records a marked change from an Eocene-Oligocene ramp to a Miocene rimmed platform (Rosleff-Soerensen et al., 2012, 2016; Howarth and Alves, 2016). The tropical Miocene sequence investigated in this work was established above a unit of temperate-water, flat-topped bryozoan reefs (Belde et al., 2017; Van Tuyl et al., 2018). Most understanding of this Miocene carbonate sequence comes from regional analyses by Rosleff-Soerensen et al. (2012, 2016), Saqab and Bourget (2015) and Belde et al. (2017). Yet, little is known about the patterns of growth within individual carbonate build-ups on the North West Shelf.

This work applies seismic stratigraphic methods to the high-resolution Poseidon three-dimensional (3-D) seismic volume, so that we provide further insights into the Miocene evolution of the Browse Basin and North West Shelf (Fig. 1). Later, this paper investigates the impact of sea level and tectonics on seismic facies in the Browse Basin, by incorporating outcrop data from the Cariatiz Reef in southeast Spain (Fig. 2). Miocene carbonate units from southeast Spain have been previously used as analogues for offshore Australia (Kleipool et al., 2017). We chose the age-equivalent Cariatiz Reef as an outcrop analogue for the Browse Basin build-ups because the clinoform bodies of both systems were produced by tropical carbonate factories (Kleipool et al., 2017). The Cariatiz reef also displays seismic-scale geometries of similar dimensions to the Browse Basin. In summary, the research questions addressed in this paper include:

1. How definite is the relationship between Miocene reef evolution, sea level and tectonics on Australia's North West Shelf?

* Corresponding author.
E-mail address: vantuylj@cardiff.ac.uk (J. Van Tuyl).

https://doi.org/10.1016/j.marpetgeo.2018.02.034
Received 11 October 2017; Received in revised form 16 February 2018; Accepted 24 February 2018
Available online 01 March 2018

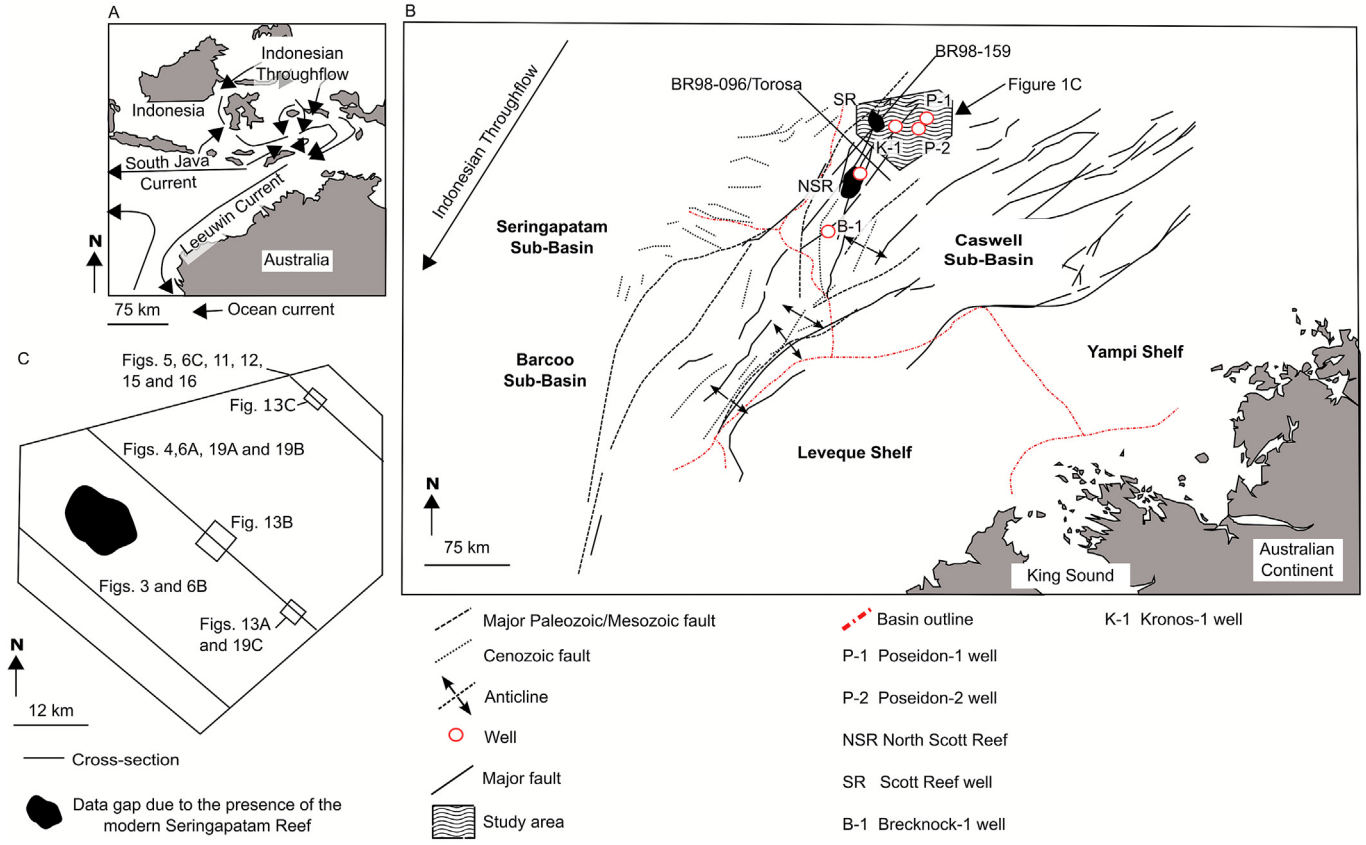

Fig. 1. (A) Regional map showing the location of the study area relative to northwest Australia, Timor Trough, and the orientations of major oceanographic currents. Adapted from Blevin et al. (1998), Struckmeyer et al. (1998) and Rosleff-Soerensen et al. (2016). (B) Map of the Browse Basin showing the location of the Caswell and Barcoo sub-basins and main northeast-striking structural trends, as well as the location of the Poseidon 3D seismic survey and key exploration wells. Adapted from Blevin et al. (1998), Struckmeyer et al. (1998) and Rosleff-Soerensen et al. (2016). (C) Regional extent of the Poseidon 3D seismic survey and locations of key profiles and variance time-slices in this paper. The position of the modern Seringapatam Reef is highlighted in the figure.

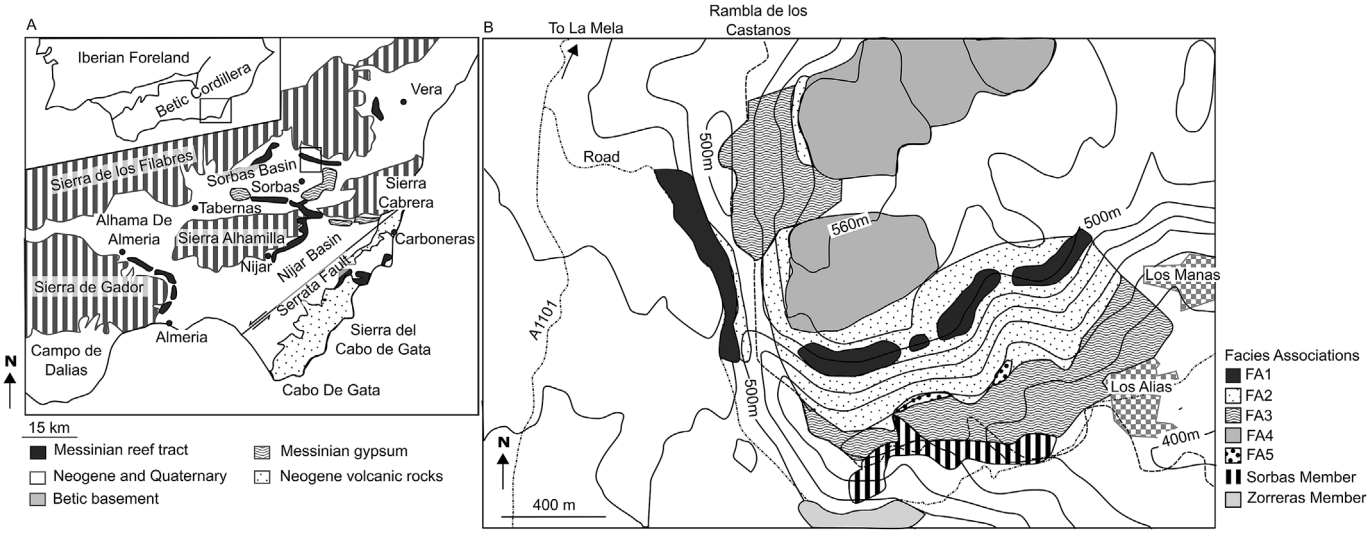

Fig. 2. (A) Regional map showing the location of the Cariatiz Reef in the Sorbas Basin, southeast Spain. (B) Location map of the Cariatiz Reef highlighting the distribution of interpreted facies associations. The field study area is located west of the village of Los Alías, northeast of Sorbas. Facies mapping identified six (6) facies associations in the outcrops of the (Miocene) fringing reef unit. FA1 comprises the reef framework. FA2 marks talus slope facies comprising reef-framework blocks and breccias. FA3 comprises basinal facies. FA4 represents lagoonal facies. FA5 represents lowstand debrites.

2. How do seismic scale interpretations of carbonate build-ups compare to outcrop scale interpretation?
3. Are seismic attribute analyses a valid method to characterise karst systems on carbonate platforms?

2. Geological setting

2.1. Meso-Cenozoic evolution of the North West Shelf

The Browse Basin is an offshore sedimentary basin on Australia's North West Shelf, itself a northeast-striking rifted continental margin (Rosleff-Soerensen et al., 2012, 2016; Stephenson and Cadman, 1994) (Fig. 1). Located on the southeast edge of the Timor Sea, the Browse Basin exhibits a series of half-grabens that strike parallel to the margin and dip landwards (Struckmeyer et al., 1998; Rosleff-Soerensen et al., 2012).

Jurassic continental rifting between Greater India and Western Australia (Kaiko and Tait, 2001; Veevers and Cotteril, 1978; Rosleff-Soerensen et al., 2012, 2016; Langhi and Borel, 2007) developed the prominent northeast-striking structural trends of the North West Shelf and Browse Basin (Bradshaw et al., 1994; Keall and Smith, 2004; Langhi and Borel, 2007; Longley et al., 2002) (Fig. 1). This rift-related topography was buried by an Early Cretaceous passive-margin sequence (Stephenson and Cadman, 1994; Langhi and Borel, 2007; Rosleff-Soerensen et al., 2012; Struckmeyer et al., 1998).

Seafloor spreading in the Indian and Southern Oceans caused northward migration of the Australian plate from ~40° south in the Oligocene/Eocene to ~20° south at present (Hull and Griffiths, 2002; Rosleff-Soerensen et al., 2012). In parallel, anti-clockwise rotation of the Australian continent during Late Oligocene-Early Miocene oblique collision between the Pacific and Australasian plates (Baille et al., 1994; Rosleff-Soerensen et al., 2012; Veevers and Powell, 1984), resulted in shallow extensional faulting and subsidence along the outer North West Shelf (Stephenson and Cadman, 1994; Howarth and Alves, 2016). Synchronous reactivation of Jurassic (and older) faults exaggerated Jurassic structures (Harrowfield and Keep, 2005; Rosleff-Soerensen et al., 2012), and generated moderate tectonic inversion in the Browse Basin (Keep et al., 2000).

2.2. Regional stratigraphy and Miocene carbonate platforms of the Browse Basin

In the study area, Cenozoic units mostly comprise carbonate strata (Rosleff-Soerensen et al., 2012, 2016). Eocene to Upper Miocene units record a transition from a ramp to a rimmed platform (Apthorpe, 1988; Rosleff-Soerensen et al., 2012, 2016; Howarth and Alves, 2016; Belde et al., 2017; Tesch et al., 2018). The regional unconformity marking the Oligocene-Miocene boundary records a sharp transition from intermediate-ramp to shallow-marine environments, and resulted in the erosion of the inner-ramp top (Stephenson and Cadman, 1994; Saqab and Bourget, 2015).

To the south of the study area, Rosleff-Soerensen et al. (2012, 2016) and Belde et al. (2017) interpreted a basinward migration of carbonate deposition from the latest Burdigalian-Langhian to the early Tortonian, an event resulting in the formation of an extensive barrier reef system along the basin margin. Subsequent sea-level rise (and associated depositional facies' retrogradation) from late Tortonian to latest Messinian broke the large barrier reef into smaller isolated carbonate build-ups, which became restricted to the top of inversion anticlines (Rosleff-Soerensen et al., 2012, 2016). However, this rapid retrogradation, interpreted in the literature as resulting from sea-level rise (Rosleff-Soerensen et al., 2016), contradicts the widely documented Late Tortonian to Messinian eustatic lowstand (Zachos et al., 2001; Haq et al., 1987; Haq and Al-Qahtani, 2005). Rosleff-Soerensen et al. (2016) linked the latest Miocene sea-level rise in Northwest Australia to elevated subsidence rates caused by the collision of the Australian and Eurasian plates at this time.

2.3. The Cariatiz Reef (SE Spain)

The Cariatiz Reef developed at the end of the Miocene in the Sorbas Basin, southeast Spain (Fig. 2). Strong subsidence from the Tortonian to the early Messinian was followed by early Pliocene-Holocene tectonic uplift, which ended marine deposition and resulted in the exposure of a 700 m-thick basin fill (Martín and Braga, 1994). The Sorbas Basin thus comprises Middle Miocene to Holocene sediments separated by major unconformities (Martín and Braga, 1994). At present, it forms a small, east-west trending, intra-montane depression surrounded by basement relief of the Betic mountain range (Fig. 2).

The unit of interest to this work is the Messinian fringing reef, one of a series of carbonate platforms that rimmed the Sorbas basin in the latest Miocene (Reolid et al., 2016) (Fig. 2). The reef overlies the Azagador member, a unit of regional expression marking the Tortonian-Messinian boundary (Ruegg, 1964), and precedes the Messinian evaporitic sequence (Martín and Braga, 1994; Braga and Martín, 1996). The Cariatiz reef lies just north of the village of Los Alías on the northern margin of the Sorbas Basin (Fig. 2).

3. Data and methodology

3.1. 3-D seismic dataset

This work uses the 2828 km^3 Poseidon 3-D seismic volume, shot between late 2009 and early 2010 (Fig. 1). It images Middle Jurassic to Holocene formations at a target depth between 1500 m and 5500 m, and is located on the Browse Basin's shelf margin, North West Australia (Fig. 1). The seismic survey comprises 172 prime sail lines and 21 orthogonal lines in the area adjacent to the Seringapatam reef (Fig. 1). It was acquired perpendicularly to the northwest-striking continental shelf and is not aligned with the long axis of fluid-venting structures or any karst networks. Therefore, no spatial aliasing issues are expected when imaging shallow features (Ho et al., 2012; Howarth and Alves, 2016).

The source used during acquisition comprised two airguns with a 10-streamer receiver set up with a spacing of 75 m (ConocoPhillips, 2012). Based on sonic data from the Poseidon-1 and Kronos-1 wells, the lower Miocene sequence has an average velocity of 3407 m/s and, therefore, a vertical resolution of 16.4 m.

The interpreted dataset follows the SEG European polarity convention, i.e. a positive amplitude marking an increase in acoustic impedance is represented as a red reflection or peak. It includes the exploration wells; Poseidon-1 Poseidon-2 and Kronos-1 (Fig. 1). Well Poseidon-1 was a wildcat and found gas in the Plover Formation, providing gamma ray and rates of penetration from 494 to 5058 m true vertical depth sub-sea (m TVDSS), resistivity data from 560 to 5058 m TVDSS, and velocity data from 2299 to 4975 m TVDSS (ConocoPhillips, 2011a). The Poseidon-2 appraisal well was drilled after the Poseidon-1 discovery to assess the presence and quality of gas in the Plover Formation (Fig. 1). It provides gamma ray and resistivity data from 556.9 to 5334.4 m TVDSS, velocity data from 2407.2 to 4702.2 m TVDSS lithologies from 2010 m TVDSS to 4053 m TVDSS (Howarth and Alves, 2016). The Kronos-1 well was also drilled to test for hydrocarbons within the Plover Formation. It provides formation top, gamma ray and resistivity data from 594.6 m TDVSS, as well as sonic velocity from

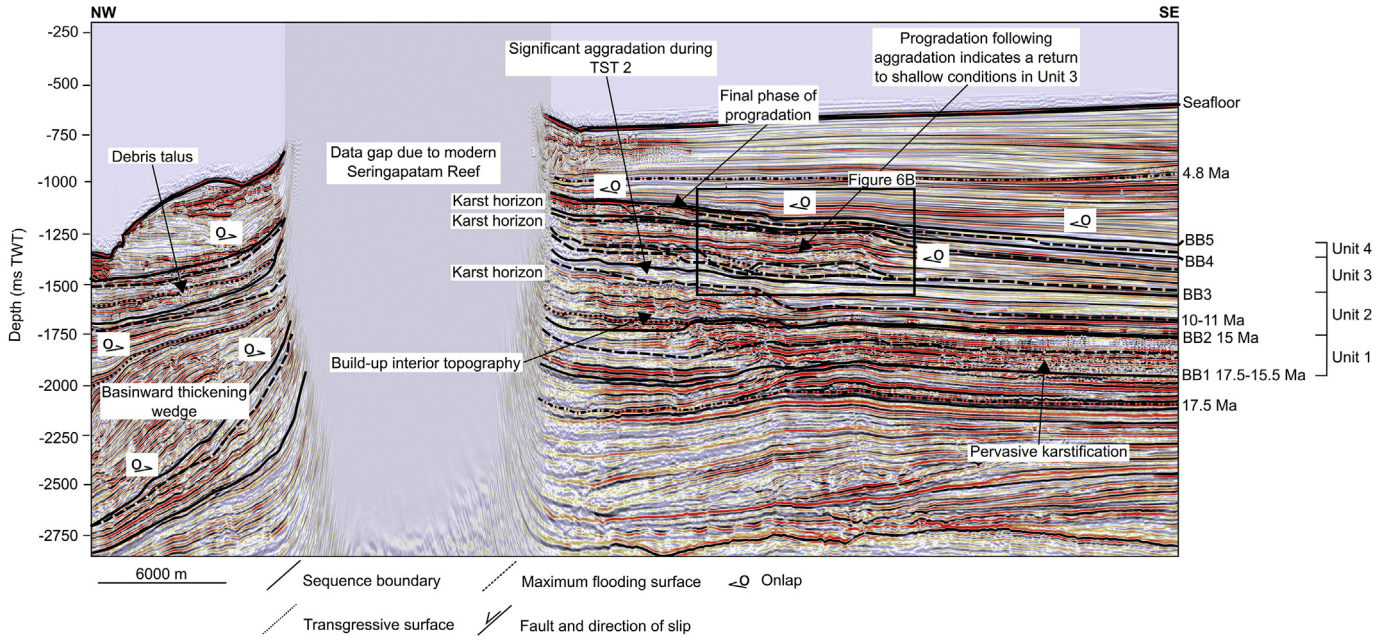

Fig. 3. Interpreted seismic profile showing the four (4) seismic-stratigraphic units of the Miocene carbonate sequence, Browse Basin. Sequence boundaries, and other key sequence stratigraphic surfaces, are also shown. Carbonate build-ups were initiated above the flat-topped Bryozoan build-ups identified by Belde et al. (2017) and Van Tuyl et al. (2018) in strata below BB1. The presence of the modern Seringapatam Reef is marked by a data gap. Above BB3, lowstand conditions allowed build-up development away from the platform, with evidence for step-out and step-down geometries on the southeast margin. These geometries correlate with a karst interval to the northwest.

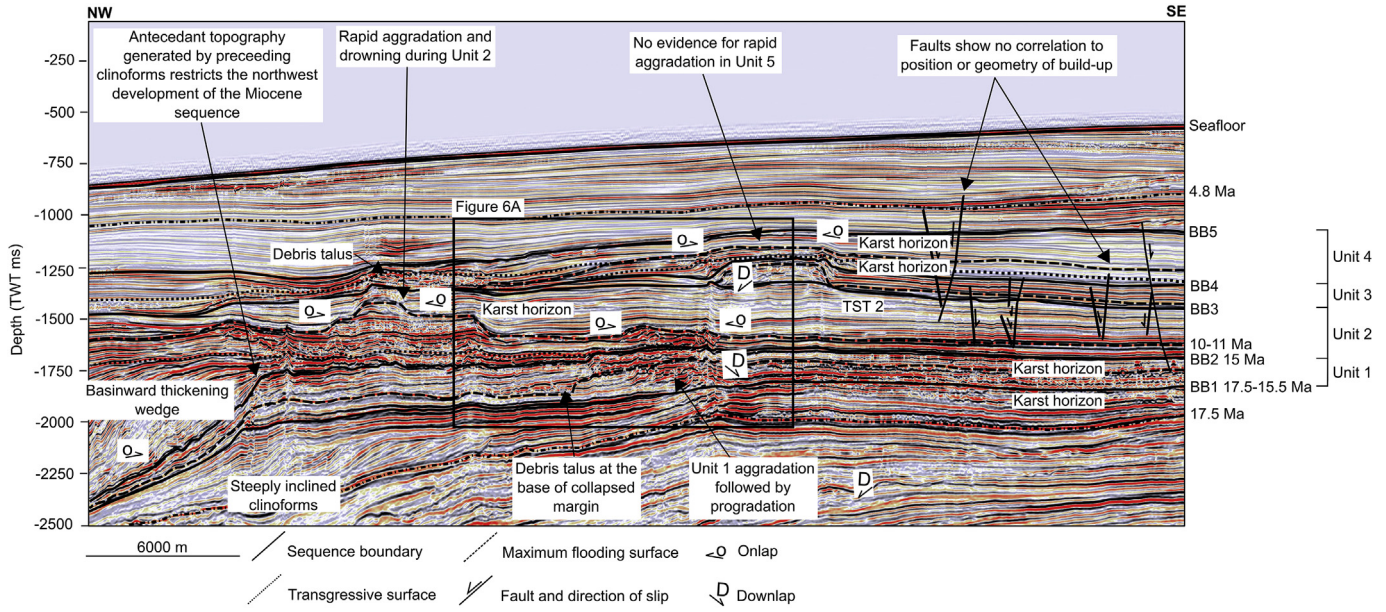

Fig. 4. Interpreted seismic profile showing the four (4) seismic-stratigraphic units of the Miocene carbonate sequence, Browse Basin. Sequence boundaries, and other key sequence stratigraphic surfaces, are also shown. Initial aggradation is followed by basinward progradation, which is restricted by antecedent topography and characterised by discontinuous reflections marking karst intervals to the southeast. Aggradation during TST 2 (see upper part of Unit 2) forced progressive margin retreat, with the build-ups being onlapped and buried by lower amplitude seismic facies. A large debris talus indicates lowstand conditions above BB3.

594.6 to 2033 m TVDSS and 2663–4778 m TVDSS (ConocoPhillips, 2011b).

In this work, the 981 m-thick Oliver limestone formation (Miocene) was divided into seismic-stratigraphic units based on the identification and mapping of sequence boundaries (see Van Wagoner et al., 1988; Schlager, 1992; Handford and Loucks, 1993; Chang et al., 2017) (Figs. 3–6). This method divides a carbonate build-up into genetically-related stratigraphic units deposited during specific phases of a relative sea-level cycle (see also Posamentier et al., 1988). Thus, it documents changes in accommodation space and sediment supply (Schlager,

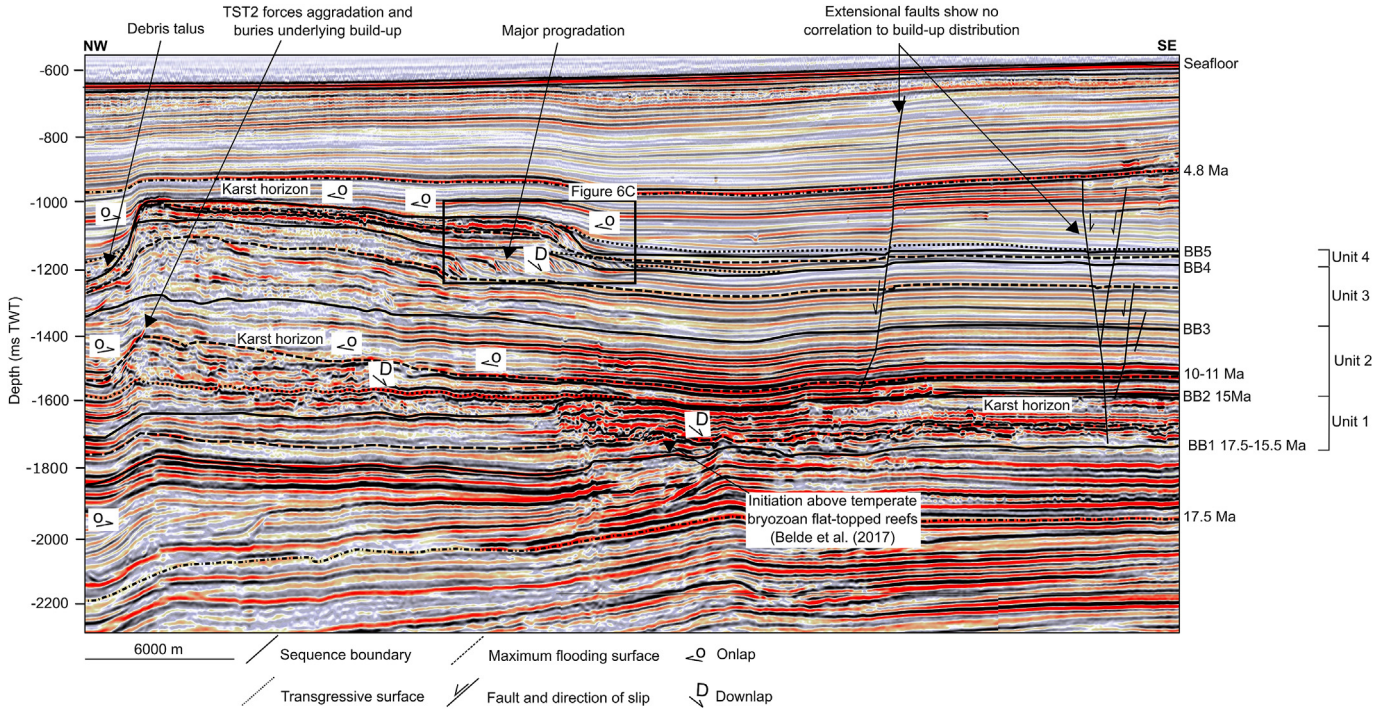

Fig. 5. Interpreted seismic profile showing the four (4) seismic-stratigraphic units of the Miocene carbonate sequence, Browse Basin. Sequence boundaries, and other key sequence stratigraphic surfaces, are also shown. Growth patterns in Unit 3 and Unit 4 are characterised by episodes of aggradation and progradation, with progradation extending the margin significantly to the southeast towards the top of Unit 3. This progradation is accompanied by karst intervals and debris talus deposits. In contrast, Unit 4 does not exhibit significant platform thickening, being characterised by progradation only towards its top. Build-ups are then onlapped and buried, with no evidence for aggradation under a transgressive systems tract. Growth patterns suggest differential accommodation-space creation between Units 3 and 4.

2005). In addition, a number of time-structural and isochron thickness maps were generated for key seismic units (Figs. 7–10).

To date sequence boundaries and seismic stratigraphic units, we used key seismic markers determined from biostratigraphy data provided by the North Scott Reef-1 well to the southwest (Fig. 1). Belde et al. (2017) estimated absolute ages using the Gradstein et al. (2012) timescale and we used the BR98-096 2D seismic line to correlate their study area with strata imaged by the Poseidon 3D seismic volume (Fig. 1B).

3.2. Velocity-depth conversion

In order to determine true depths of mapped horizons, and thus accurate dip angles for seismic reflections in the interpreted carbonate build-ups, velocity data from the Kronos-1 well-completion report (ConocoPhillips, 2011b) were used to time-depth convert the 3-D seismic volume (Table 1). The Kronos-1 well provided an average interval velocity of 3407 m/s for the Miocene Oliver Formation strata. The time depth conversion was completed on Petrel® and based on the equation:

$$\text{True Depth} = ((\text{TWT depth} / 2) / 1000) * \text{velocity} \quad (1)$$

3.3. Seismic facies and attribute analyses

Seismic reflection analyses (Fig. 11A and Table 2) were based on Bachtel et al. (2004), who used seismic reflection geometry and the location of reflections within carbonate platforms to predict seismic facies offshore Indonesia. Seismic attributes used in this study include local structural dip attributes (event dip) (Fig. 11B). The use of dip attributes builds upon the work of Kenter (1990), who studied twenty (20) ancient carbonate platforms and provided a correlation between the angles of repose for sediment and different (carbonate) facies. The dip attribute returns the downslope dip of a seismic reflection, in which the gradient is assumed to be perpendicular to the seismic event. In essence, the dip attribute comprises an edge detection method revealing rapid changes in the local dip (e.g. fractures) on 3-D seismic volumes (Koson et al., 2014). Hence, it can also be used to outline reflection geometry in seismic geomorphological interpretations (Koson et al., 2014).

In this work, the structural dip attribute was applied to the depth-converted seismic volume. Quality control of the extracted dips was attained through manual calculation by sub-dividing individual seismic reflections along their profile where there was a visible change in dip angle. Using the trigonometry function, seismic reflections were treated as right angle triangles - the opposite and adjacent sides of the triangle were measured and included in Equation (2):

$$\text{Slope angle} = \tan^{-1} (\text{Opposite} / \text{Adjacent}) \quad (2)$$

Instantaneous phase reveals the continuity of seismic reflections that vary greatly in amplitude (Fig. 11C). It is calculated on a sample-by-sample basis with no regard for waveform. As such, it is a good indicator of continuous features, faults, pinch-outs, bed interfaces, sequence boundaries, and regions with onlapping reflection patterns.

Instantaneous frequency, which is the time derivative of phase, is calculated from the temporal rate of change of the instantaneous phase (Fig. 11D). Instantaneous frequency is a useful tool for identifying and estimating seismic attenuation caused by oil and gas reservoirs, i.e.

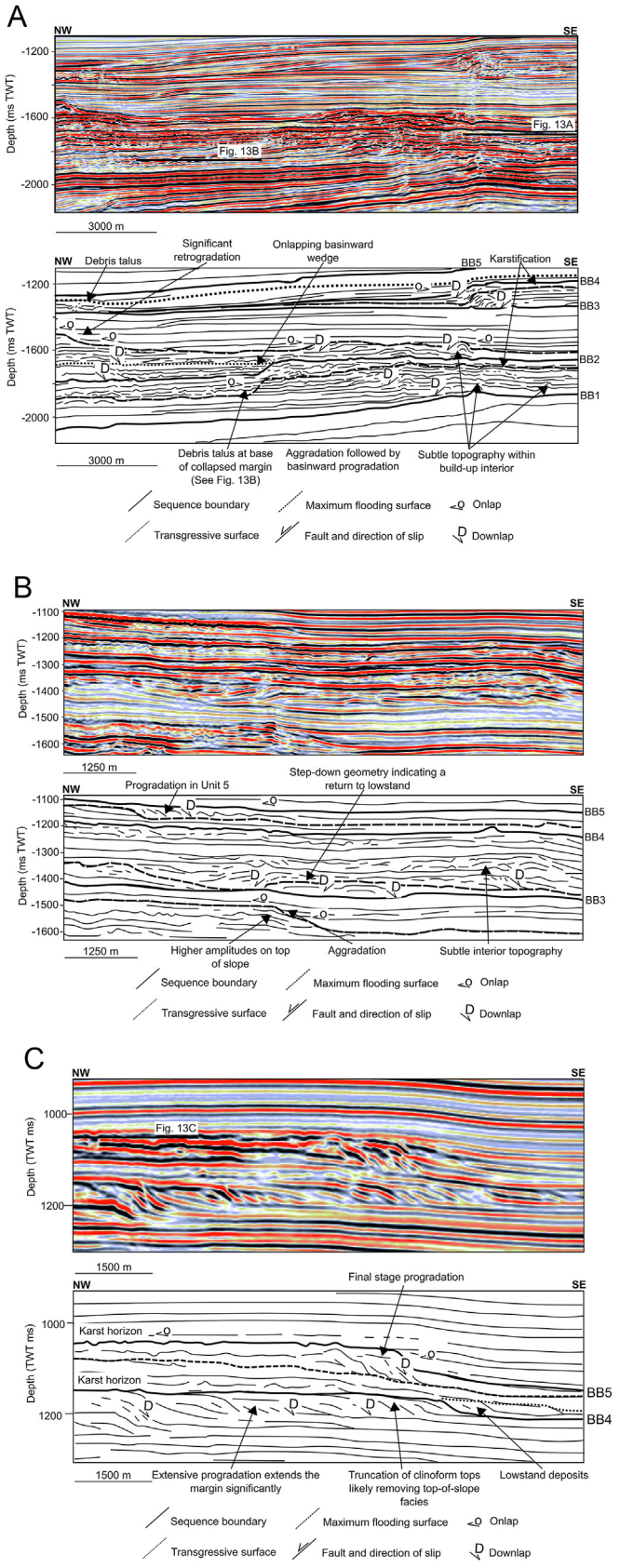

Fig. 6. (A) Zoomed in seismic profile from Fig. 4 and corresponding line drawing showing growth geometries in Unit 1. Downlapping geometries mark the initial phase of aggradation in Unit 1. Seismic reflections to the southeast are discontinuous and represent karst intervals. Subsequent reflections exhibit basinward progradation of approximately 3 km. The northwest margin of this progradational phase is marked by a sharp margin with debris at the toe of the slope (See Fig. 13B). Above BB2 seismic reflections show downlapping geometries and subtle topography. Moving upwards through Unit 2, build-ups are observed to aggrade and are onlapped by parallel seismic reflections. Above BB3, seismic reflections downlap onto this sequence boundary. Clear progradational geometries are observed. (B) Zoomed in seismic profile from Fig. 3 and corresponding line drawing. Below BB3, the aggradational phase of Unit 2 is clearly visible. Seismic reflections downlap onto BB3, showing alternating phases of aggradation and progradation. A transgression is observed at the top of Unit 3, with the build-up margin retreating to the northwest before building up to the southwest again. Another phase of aggradation is observed above BB4 before a final phase of progradation. (C) Zoomed in seismic profile from Fig. 5 and corresponding line drawing. Progradational geometries are observed below BB4, and extend the margin over 3 km to the southeast. Clinoforms show clear truncation at the top of the slope. Retrogradation is observed above BB4 before the margin builds out again to the southeast and develops prograding clinoforms just below BB5.

fluid accumulations causing local drop-offs in high-frequency components. It is also useful for measuring the cyclicity of geological intervals and for cross-correlating strata across faults (Marfurt and Alves, 2015).

Variance quantifies the differences between a given seismic trace and its neighbours (Fig. 13). It highlights discontinuities inside or in between seismic reflections, i.e. the physical reasons for high variance, displaying at the same time subtle stratigraphic features (e.g. karsts and faults) (Omosanya and Alves, 2013).

3.4. Fieldwork methods

Fieldwork comprised the mapping of geometries and facies distributions across the Cariatiz Reef, southeast Spain (Figs. 2 and 14). Facies associations were identified using the Dunham classification (Dunham, 1962). Angles of repose for clinoforms were measured systematically along discrete reef depositional facies so as to identify any trends between facies associations and these same angles of repose (Fig. 14B). The present-day tectonic tilt of the Cariatiz Reef, adding 1.6° to the observed direction of progradation in clinoforms (Braga and Martín, 1996), was taken into consideration during the field measurements. Structural features (faults, fractures, and karsts) were documented in great detail. Field data were used to aid the interpretation of seismic geometries and facies associations offshore northwest Australia.

4. Results

4.1. Seismic-stratigraphic units

Miocene strata in the Browse Basin were sub-divided into four (4) seismic units (Figs. 3–5). Two major sequence boundaries include BB1, which marks the top of the Eocene-Oligocene ramp at 2789 m (1796 ms TWT) and BB5, marking the top Miocene in the Poseidon-2 well at 1808 m (1142 ms TWT). Both surfaces are local unconformities with important karstification (Figs. 3–5 and 6A).

4.1.1. Unit 1: Aquitanian to Langhian (17.5–15.1 Ma)

Unit 1 is laterally continuous across the interpreted seismic volume (~62 km) and forms above sequence boundary BB1 (Figs. 3–5, and 6A). This boundary is characterised by pervasive, discontinuous seismic reflections that generate circular to sub-circular high-variance

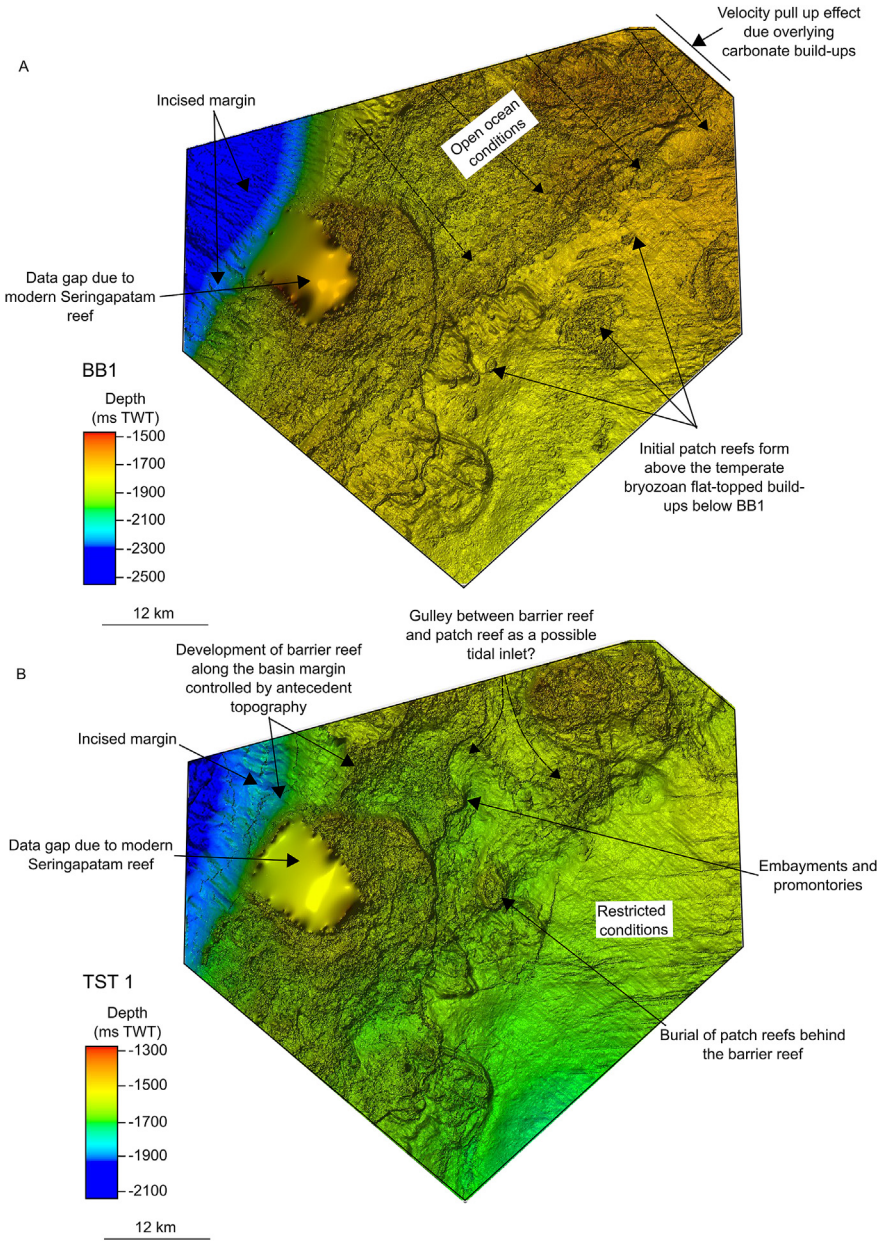

Fig. 7. (A) Two-way-time depth map of sequence boundary BB1. Topography prior to the Miocene initiation of carbonate build-ups shows flat-topped bryozoan reefs (see Belde et al., 2017), and a sharp break in slope to the northwest (see also Van Tuyl et al., 2018). This break in slope is regularly incised and controls the northwesterly extent of the Miocene carbonate sequence. Circular to sub-circular topographic highs represent carbonate build-ups with a patch-reef morphology (B) Two-way-time depth map of TST1. Topographic highs mark the location of carbonate build-ups. Following Unit 1, the carbonate system moves progressively to the basin margin and develops a northeast-trending build-up, controlled by the preceding break in slope. This build-up is widest in the southwest and thins to the north. Evidence for a break in the barrier reef is shown by a depression separating it from a build-up to the northeast. This suggests that relatively open ocean conditions affected the interior lagoon, hence the appearance of small patch reefs above TST 1.

depressions (Figs. 3–5 and 6A). Aggradational seismic reflections within Unit 2 (Fig. 6A) develop a ~62 km northeast-striking positive topographic feature. This feature shows variable amplitude and is backed by high-amplitude reflections, which show subtle topography (Fig. 6A). The high-amplitude reflections develop a discontinuous character to the southeast, as expressed by the presence of pervasive high-variance circular to sub-circular depressions, some of which can be up to 250 m in diameter in variance time slices (Fig. 13a).

Unit 1 shows marked progradation (< 5 km) to the southeast of the study area, a character enhancing build-up margin topography (Figs. 5–7). Onlapping geometries are observed in this area together with seismic reflections that show a parallel, highly discontinuous character. Pervasive circular to sub-circular depressions with high variance are observed in this same region (Figs. 5–7 and 8A).

A package of chaotic seismic reflections onlaps the base of slope of the northeast-trending build-up (Figs. 6A and 13B). Variance time slices show these deposits to comprise rectangular blocks over 500 m in length, which collectively form lobe-shaped geometries that are laterally continuous along the build-up margin (Fig. 13B). Unit 1 is capped by BB2 (Figs. 3–5 and 6A).

4.1.2. Unit 2: Langhian to Tortonian (15-11 Ma)

A basinward thickening wedge onlaps BB2 in the study area (Figs. 3–5). Its margin is incised by narrow northwest-striking, linear depressions (Fig. 7B), with chaotic seismic reflections occurring downslope from this same margin. Above these chaotic strata, seismic reflections exhibit downlapping geometries and variable amplitude (Fig. 6A), developing a 54 km-long northeast-striking build-up on the basin margin, approximately 22 km northwest of Unit 1 (Figs. 7B and 8A). Unit 2 widens from 6 km to 27 km to the southwest. The southeast

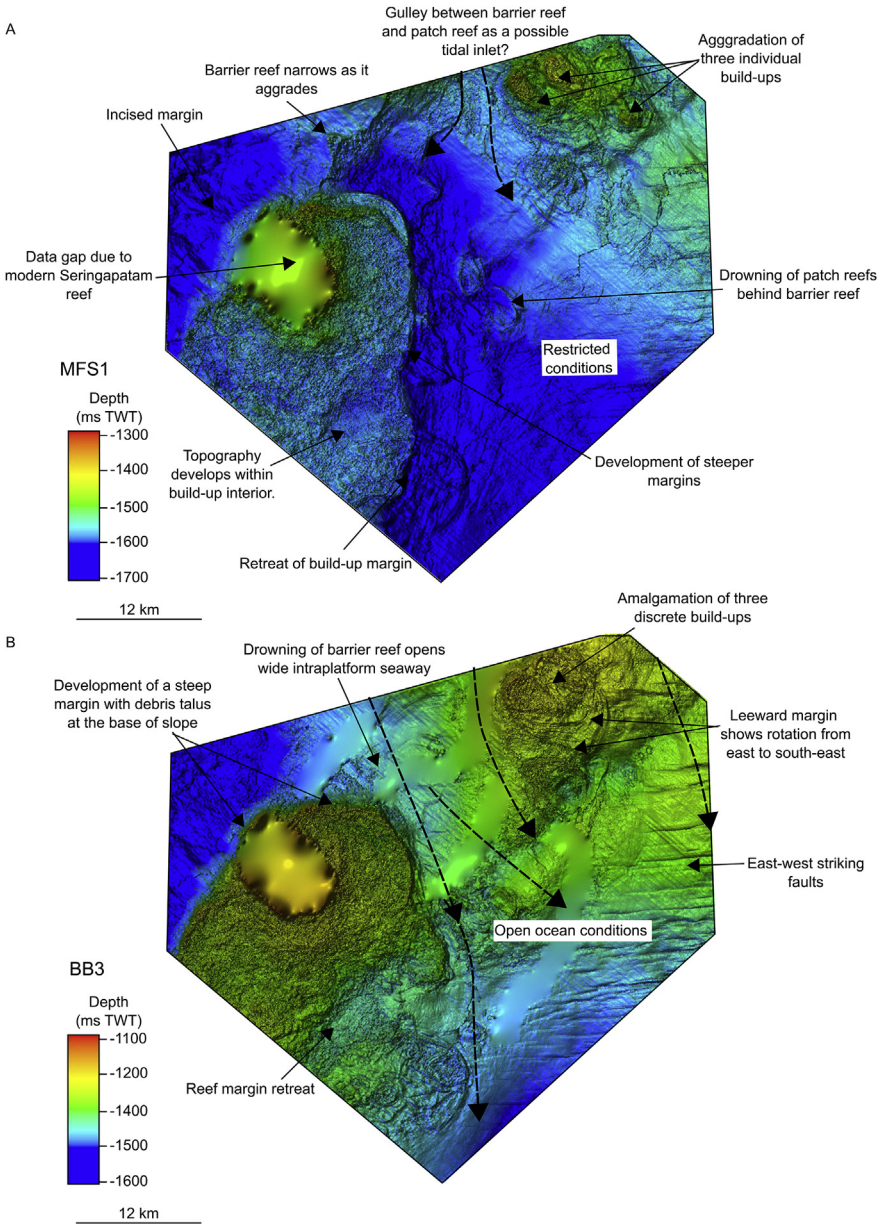

Fig. 8. (A) Two-way-time depth map of MFS 1. Aggradation in Unit 2 generated prominent margins and caused margin retreat in all carbonate build-ups, with topographic highs marking focal points of aggradation. In such a setting, topographic lows within build-up interiors are indicative of marine incursions. Patch reefs within the interior lagoon to the east were also drowned. (B) Two-way-time depth map of BB3. Prolonged aggradation resulted in significant margin retreat on the southeast margins. The barrier reef was then drowned and buried, likely establishing open-ocean conditions across the southeastern part of the study area. Southwest striking faults are observed in the east of the study area, but show no correlation with the location of carbonate build-ups.

margin shows numerous embayments and promontories, while its northwest margin is linear with only one promontory (Fig. 8B).

A second sub-circular build-up, ~15 km wide, develops northeast of the basin margin build-up (Fig. 8A). Seismic reflections to the southeast of the basin margin build-up have a subtle discontinuous character along the underlying topography, which is onlapped by parallel seismic reflections.

Aggradational geometries are persistent through most of Unit 2, causing significant platform thickening (Fig. 6A and B). Build-up margins show back-stepping of ~1 km during the top of Unit 2 (Fig. 6B). The build-ups are progressively onlapped by low-amplitude, parallel seismic reflections (Fig. 6A and B). Progressive onlap eventually buries the build-up running along the basin margin (Fig. 8B). Locally, aggradation persists in the form of small isolated build-ups in the northeast and southwest of the study area. The top of Unit 2 is marked by a third sequence boundary (BB3).

4.1.3. Unit 3: Tortonian to earliest Messinian (11.1–7.26 Ma)

Locally, aggradational seismic reflections downlap onto Unit 2 and BB3 (Figs. 3–5, and 6B). Intervals with chaotic seismic reflections are observed at the base of Unit 3 around the large build-up in the southeast (Fig. 3). Unit 3 shows an increase in the number of isolated build-ups, with new build-ups being now separated by seaways formed to the southeast of the build-up that persisted during Unit 2 (Fig. 9A). Towards the top of Unit 3, progradational geometries extend the build-up margins up to 6 km to the southeast (Fig. 6C). This caused coalescence between isolated build-ups to the southeast of the largest one, forming a hook-shaped carbonate build-up (Fig. 9B). Compared to Unit 2, carbonate build-ups in Unit 3 exhibit steeper margins on their western, northwestern, and northern margins and are circular to sub-circular, elongated in a southeast direction (Figs. 7–9). Following progradation, chaotic seismic reflections with high variance, thickening downslope, are observed on the southwest margins of some build-ups (Figs. 9A and

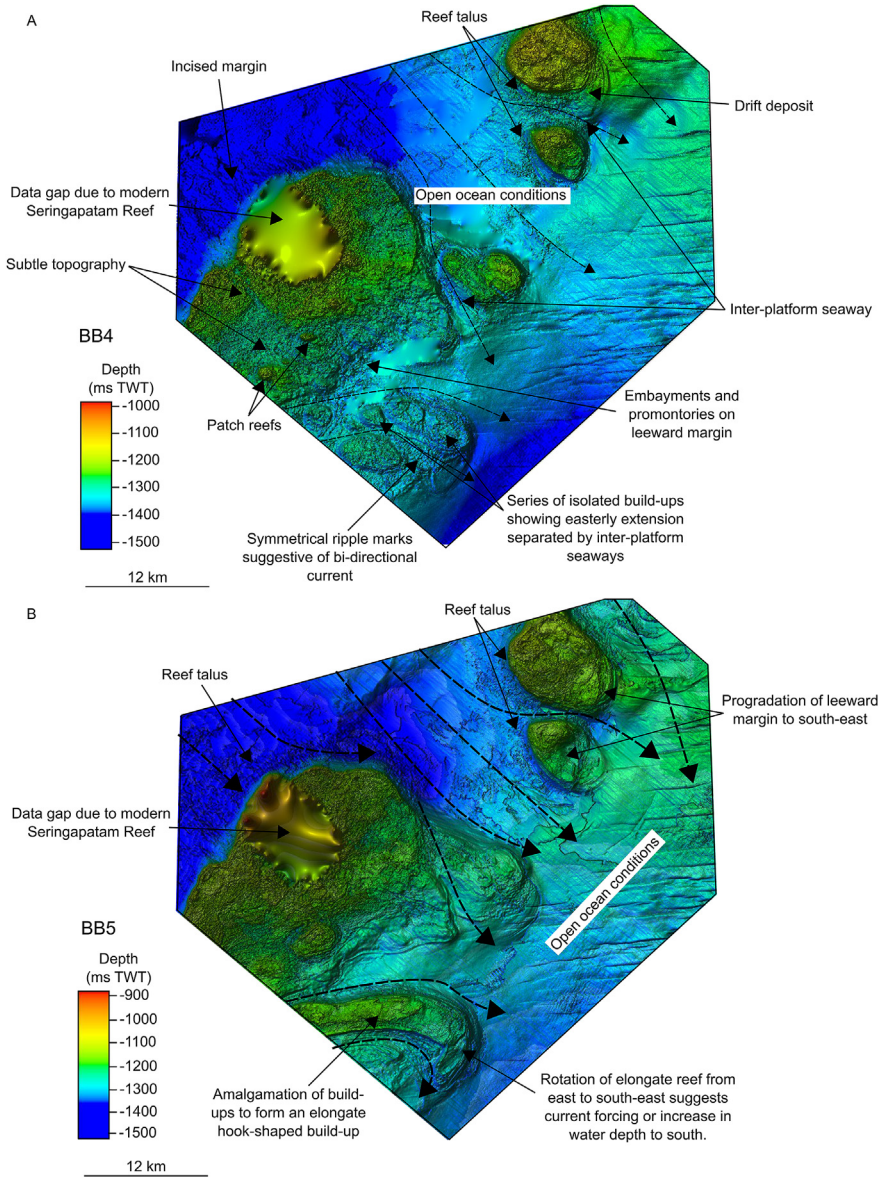

Fig. 9. (A) Two-way-time depth map of BB4. Following aggradation, isolated patch reefs became dominant. New build-ups were established o the margins of those persisting in Unit 2. Initial growth was predominantly by aggradation and, consequently, build-ups thickened and developed pronounced margins. Intra-platform seaways were established between build-ups, and evidence exists for large-scale ripples in the southern part of the study area. The orientation of intra-platform seaways indicates that currents were wrapping around the northwest build-ups and shaping their southeast margins. (B) Two-way-time depth map of BB5. Progradation resulted in amalgamation between build-ups to the south, to form a prominent hook shaped build-up. Build-ups to the north prograded to the southeast, with build-ups developing an ellipsoid geometry towards the southeast.

11A). Upslope, there is evidence for fringing reefs, and build-up interiors develop discontinuous seismic reflections with high-variance, and circular to sub-circular depressions (Figs. 11A and 13C). This marks a fourth sequence boundary (BB4) at the top of Unit 3 (Figs. 3–5).

4.1.4. Unit 4: Messinian (7.26 to > 4.8 Ma)

Unit 4 is initially characterised by aggradation and carbonate build-ups onlapped by low-amplitude strata (Fig. 6C). The margins of carbonate build-ups backstep as much as 6 km in the SE, resulting in the burial of the hook-shaped reef observed in Unit 2 (Fig. 19B).

The final phase of Unit 4 is marked by progradation extending the margins of all carbonate build-ups to the southeast by a maximum of 1.2 km (Fig. 6C). Internal seismic reflections in the build-ups are highly discontinuous, producing high-variance, circular to sub-circular depressions. The subtle chaotic appearance on the slope suggest the presence of a debrite (Fig. 11A). After the generation of this latter debrite, build-ups were onlapped by, and buried under, low-amplitude strata (Figs. 3–5 and 6C). Little to no evidence for aggradation is observed towards the top of Unit 4 (Fig. 11A).

5. Seismic stratigraphic interpretation

As summarised in Figs. 3–5, we identify Unit 1 as reflecting accommodation-space creation above the karstified sequence boundary BB1. Aggradation reflects a ‘catch-up’ phase under a transgressive systems tract (TST 1). The progradational geometries above TST 1 indicate a decrease in accommodation-space creation and the deposition of a highstand systems tract (HST 1). A maximum flooding surface (MFS 1) marks the base of this progradational sequence.

Following HST 1 a debrite interval (Unit 1), and the basinward thickening wedge of Unit 2, indicate relatively slow accommodation-space creation. This event facilitated karstification to the southeast under a lowstand system tract (LST 1) bounded at its base by a second sequence boundary (BB2).

Aggradational seismic reflections at the base of Unit 2, onlapping BB2, reflect fast accommodation-space creation and a prolonged ‘catch-up’ phase under a second transgressive phase (TST 2). This TST2 is capped by a second MFS (MFS 2). Base-of-slope debrites at the foot of build-ups to the south, the growth of build-ups above TST 2, and the

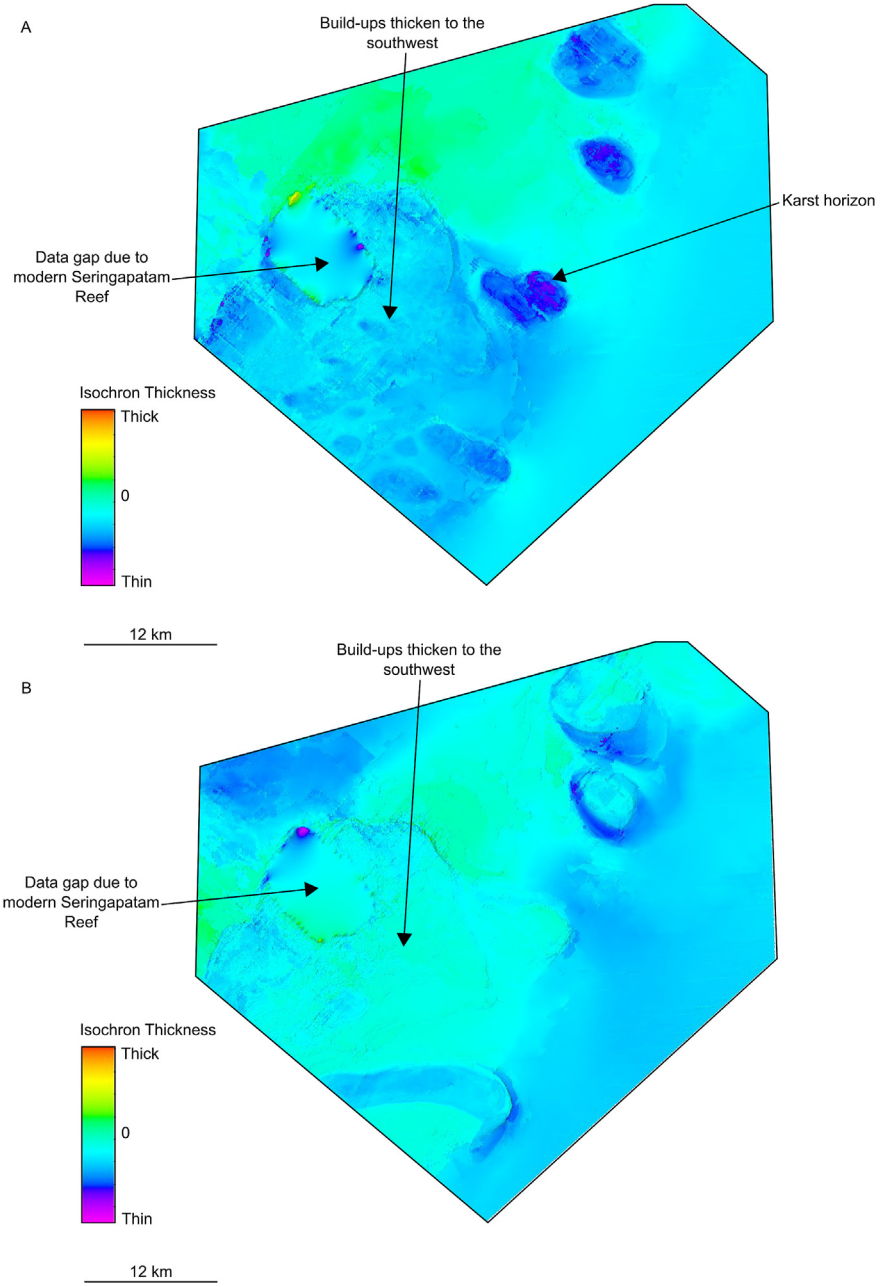

Fig. 10. Isochron thickness maps of (A) Unit 4, and (B) Unit 5. Both maps show that build-ups thicken to the southwest suggesting that accommodation-space creation was greatest in this part of the study area during the deposition of Units 4 and 5.

karstification of build-up interiors that persisted during Unit 2, suggest a loss of accommodation space at first, followed by its creation in a second stage. Consequently, we interpret sequence boundary BB3 to precede a second LST (LST 2). The subsequent aggradational phase of Unit 3 reflects accommodation-space creation and a 'catch-up' phase occurring in response to a third transgressive systems tract (TST 3). A switch to progradational geometries marks a third MFS (MFS 3), and associated loss of accommodation space under a third HST (HST 3). The overlying debris deposits at the base of the build-up margins, the karstified build-up interiors, and evidence for fringing reefs after MFS 3, mark a fourth sequence boundary (BB4) underlying a third lowstand systems tract (LST 3) (Figs. 3 and 4).

Subsequent aggradation indicates accommodation-space creation and a fourth transgressive systems tract (TST 4). Progradation at the top of Unit 4 implies a relative loss of accommodation space and the establishment of a fourth HST (HST 4). The top of Unit 4 is karstified, and there is subtle evidence for the deposition of debris deposits, suggesting a fifth sequence boundary (BB5). This was followed by LST 4 prior to drowning and burial of build-ups by low-amplitude seismic reflections under a TST 5 (Fig. 6A and B, and 6C).

Table 1
Table summarising the velocity data from the Kronos-1 well. Italics refer to members within formations where velocity data was available.

Interval	Formation	Top (MDRT)	Bottom (MDRT)	Top OWT (s)	Base time OWT (s)	Average velocity m/s
Water collumn		0	533.8	0	0.3453	1516
Pliocene	Barracouta	533.8	968	0.3453	0.5763	1879.65367965368
Miocene - Oligocene	Oliver Limestone	968	2443	0.5763	1.0093	3406.46651270208
Eocene	Prion Limestone	2443	2858	1.0093	1.1062	4282.7657378741
Eocene-Palaeocene	Grebe Limestone	2858	3675	1.1062	1.2826	4631.51927437642
Eocene-Palaeocene	*Heywood Limestone member*	*2858*	*3460*	*1.1062*	*1.2323*	*4773.98889770024*
Eocene-Palaeocene	*Baudin Marl member*	*3460*	*3675*	*1.2323*	*1.2826*	*4274.35387673956*
Palaeocene	Johnson Formation	3675	3919	1.2826	1.3448	3922.82958199357
Late Cretaceous	Woolaston Gibson Fenalon Pudhoe	3919	4046	1.3448	1.3762	4044.58598726114
Cretaceous	Jamieson	4046	4577	1.3762	1.5275	3509.58360872439
Late Jurassic	Montara	4577	4585	1.5275	1.5308	2424.24242424253
E. to M. Jurassic	Plover formation	4585	5075	1.5308	1.6374	4596.62288930582
E. to M. Jurassic	*Plover Top Volcanics*	*4585*	*4776*	*1.5308*	*1.5739*	*4431.55452436193*
E. to M. Jurassic	*Plover Top Reservoir*	*4776*	*5075*	*1.5739*	*1.6374*	*4708.66141732284*
L. Triassic	Nome	5075	5235.8	1.6374	1.6803	3748.25174825176

6. Facies associations

6.1. Outcrop facies associations in the Cariatiz Reef, Sorbas Basin

The six facies associations (FA1 to FA6) interpreted at Cariatiz are summarised in Figs. 2 and 14. FA1 to FA6 complement the descriptions in Riding et al. (1991), Martín and Braga (1994), Braga and Martín (1996) and Sanchez-Almazo et al. (2007):

a) FA1: Porites within a coarse-to very-coarse bioclastic micritic floatstone to packstone matrix. Porites abundance decreases upwards through the outcrop section. Margin parallel, m-scale cave systems are observed in FA1. Dissolution of Porites generated moldic and vuggy porosity. Fractures and spaces between Porites crusts are infilled by calcite; however, it is difficult to determine when the calcite infill was formed. Observed angles of repose are up to 7°, with an average of 5°. FA1 is interpreted to represent the reef framework in a zone of high energy located on the windward margin of the Cariatiz reef.
b) FA2: Thick clinoforms (> 10 m) with angles of repose between 14° and 41° (average 25°) comprise m-scale blocks grading downslope into cm-scale breccias sitting within a coarse rudstone to packstone matrix. The breccias reflect a decrease downslope in the size of fallen gravitational blocks and associated deposits. Blocks contain bioclasts of Porites, bivalves, serpulids and coralline algae. Blocks exhibit moldic and vuggy porosity after Porites has been dissolved. FA2 is interpreted to represent debris talus with blocks and coral breccias sourced from the reef framework.
c) FA3: Bioclastic (molluscs, coralline algae) material, abundant serpulids and Halimeda. Serpulids regularly encrust slope deposits (Braga and Martín, 1996; Reolid et al., 2016). Coarse-grained rudstones to packstones grade downslope into medium-grained packstones, which interfinger with basinal marls at the base of the slope. Locally, erosive surfaces are observed in strata belonging to this facies association. FA3 exhibits angles of repose between 5° and 16° (average 10°), and thins downslope. FA3 is interpreted to reflect the basinward transition from the debris talus to the basin floor.
d) FA4: Stratified packstones and floatstones grading locally into oyster-rich fine-grained marls in recognised depressions. Coarse-grained packstone to floatstones intervals form small topographic highs, together with coarse-grained siliciclastics. Moving towards the reef margin, floatstones and packstones containing coral fragments. Porites and coralline algae are also observed. FA4 develops angles of repose between 1° and 6°, with an average of 4°. FA4 is karstified, with cm-scale circular depressions. Karsts become more abundant around topographic highs. FA4 is interpreted to represent lagoonal facies. Topographic highs mark localised lagoonal carbonate shoals. Siliciclastic intervals represent beach deposits and fluvial units sourced from the Sierra de los Filabres to the north.
e) FA5: Stratified coarse-to very-coarse bioclastic rudstones to packstones, comprising significant shell debris within a sandy coarse-grained matrix. Discrete beds show dips varying from 11° to 15° (average 13.2°), and are up to 2 m thick. Most beds pinch-out laterally and show evidence of coarsening-upward cycles with erosive bases. They interfinger with medium sands and fine-grained marls downslope. FA5 sits between clinoforms of FA2 and is interpreted to represent lowstand sheet-fan deposits equivalent to the 'inverted wedges' described in Braga and Martín (1996) and Reolid et al. (2016). The types of shells and shell debris in FA5 indicate these are high-energy deposits sourced from the platform interior.
f) FA6: Chaotic conglomerates with angular clasts. Clasts comprise shell debris, bioclastic sandstones, Porites and oyster shells, as well as quartzite, marbles, and mica-schists within a very coarse-grained sandy matrix. Clasts of mica-schist range from m (> 2 m) to cm scales. FA6 exhibits an erosive base, and grades downslope into interbedded medium-grained sandstones and siltstones. FA6 represents high-energy debris flows sourced from the reef crest and the pre-Neogene basement of the Sierra de Filabres to the north. The scarce evidence for interbedded reef clinoforms in FA6 suggests that strata in this facies asssociation are either peri-reefal and deposited locally after a HST (or LST), or more likely comprise the post-evaporitic Terminal Complex (Sorbas Member) proposed by Bourillot et al. (2010).

6.2. Seismic facies associations

Two seismic facies associations (SF1 and SF2) can be interpreted within the Miocene carbonate sequence (Table 1). Seismic facies 1 (SF1) shows low-amplitude and variance, and laterally continuous seismic reflections of uniform thickness and amplitude (Table 1, Figs. 11 and 12). The facies is interpreted as comprising fine-grained muds, possibly interbedded with carbonate-rich sediment gravity flows close to the margins of reefs, deposited in relatively deep open-marine and carbonate-shelf settings (Fournier et al., 2005; Erlich et al., 1990).

Seismic facies 2 (SF2) refers to carbonate build-ups with high-amplitude seismic reflections, with sigmoidal to sigmoid oblique geometries (Table 1, Figs. 11 and 12). Internal seismic reflections correlate with circular to sub-circular depressions along sequence boundaries, often exceeding 60 m in diameter and exhibiting dendritic patterns (Fig. 13C). These geometries are comparable to carbonate build-ups on the North West Shelf (Rosleff-Soerensen et al., 2012, 2016; Belde et al., 2017) and Indonesia (e.g. Fournier et al., 2005; Bachtel et al., 2004). Within SF2, five seismic sub-facies are recognised (Table 1):

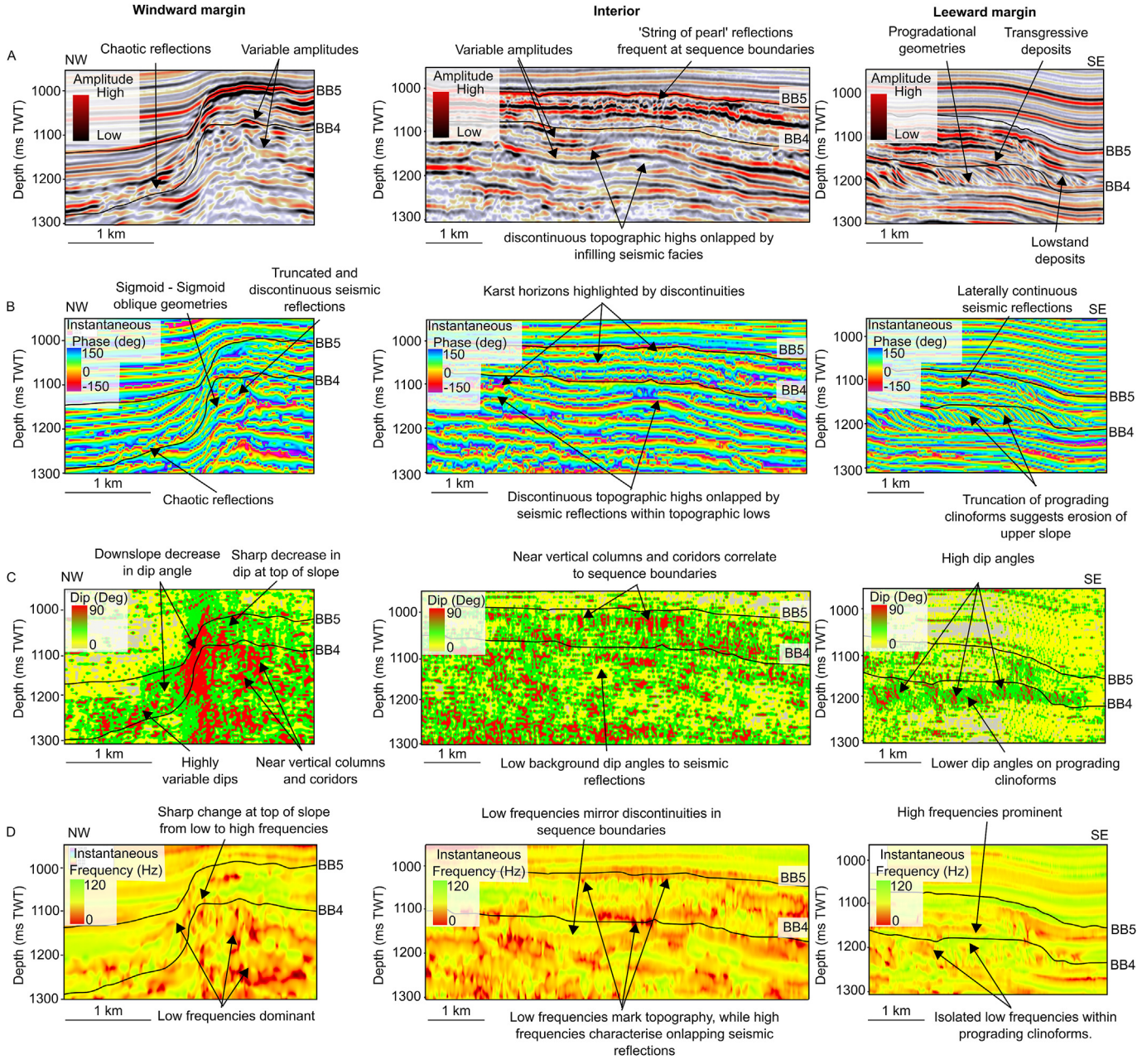

Fig. 11. (A) Seismic profile showing the amplitude and morphology of seismic reflections in a carbonate build-up. Seismic reflections show sigmoidal to sigmoid-oblique geometries on windward and leeward margins, which become truncated and highly discontinuous on the upper slope to mark the position of karsts and cave systems. Conversely, at the toe of the slope chaotic and low-amplitude strata are suggestive of debrites. Sequence boundaries are marked by discontinuous, 'string of pearl' seismic reflections indicating karst intervals associated with subaerial exposure. (B) Seismic profile showing the instantaneous phase of seismic reflections in a carbonate build-up. On both windward and leeward margins, seismic reflections are truncated and onlapped by uniform, parallel seismic reflections. Truncation of seismic reflections at the top of the slope may indicate the presence of sub-seismic debris facies on the lower slope. Seismic reflections are discontinuous on the windward margin, possibly marking the position of flank margin karsts and caves. Topographic highs within build-up interiors and associated onlapping geometries suggest the presence of lagoonal patch reefs. (C) Seismic profile highlighting the dip of seismic reflections in a carbonate build-up. Base of slope and onlapping seismic reflections exhibit low dip angles, interpreted as mud rich facies. Middle-to upper-slope seismic reflections show a progressive increase in dip at the transition from mud-supported to grain-supported facies. Windward margins exhibit higher dips than leeward margins, suggesting they have a lower percentage of mud on the upper slope (see Kenter, 1990). Near-vertical dips exhibiting column and corridor geometries are observed within the windward margin and along sequence boundaries within the build-up interior. Their locations agree with the expected positions of flank-margin and phreatic caves on the windward margin, and with karst intervals associated with sub-aerial exposure of the platform at sequence boundaries. Highly variable dips characterise debrite intervals on the lower slope. (D) Seismic profile showing the instantaneous frequency of seismic reflections in a carbonate build-up. Instantaneous frequency displays a correlation between the positions of interpreted grain-supported facies, karsts, caves and low seismic frequencies, as expected given the reservoir properties of coarser-grained facies and presence of hydrocarbons in the Browse Basin. Build-up interiors exhibit typically higher seismic frequencies, with topographic highs exhibiting low frequencies that agree with the interpretation of patch reefs in otherwise lower-energy (muddy) lagoonal environments. Leeward margins exhibit fewer 'drop-offs' in high frequency components, suggesting more uniform strata with possible reservoir potential confined to karst intervals.

Table 2
Table summarising the seismic properties of the different seismic facies identified within the Miocene sequence in the Browse Basin. Five seismic facies are observed each with different properties. Analogue facies from the Cariatiz Reef are assigned to each seismic facies.

Seismic Facies	Seismic reflection geometry	Amplitude	Dip (°)		Comments	Depositional environment	Cariatiz analogue facies
			Attribute	Manual			
SF1	Horizontal, onlapping reflections	Uniform, Low (typically around 3000)	0 to 30	< 5	Uniform low variance and high instantaneous frequencies (~60 Hz)	Deep water, basinal	None observed
SF2.1	Parallel with uniform thickness	Low (−454 to −990)	0 to 10 (up to 90 at kart horizons)	< 5	Uniform low variance and high instantaneous frequencies (~60 Hz)	Toe of slope	FA3
SF2.2	Variable thickness. Concave in lower slope to inclined in upper slope. Form packages of sigmoid to sigmoid oblique seismic reflections. Top of reflection often truncated.	Upslope change from medium to high (−1175 to −4741)	10 to 80	05/45	Drop-offs in high frequency components (~20 Hz). Reflections thicken up-slope. Locally discontinuous, generating high variance, high dip angle features which do not always conform with sequence boundaries.	Slope	FA2 and FA3
SF2.3	Mark sharp drop in angle of repose at top of slope. Parallel but commonly sho pervasive discontinuity. Localised topograhpy.	Variable (−1052 to −10 528)	0 to 10 (up to 90 at kart horizons)	< 10	Sharp decrease in angle of repose at top of SF2.2. Often truncate clinoforms. Interior topography is onlapped by lower amplitude seismic reflections. High dip angle columns at sequence boundaries and windward margins conform to high variance karsts.	Lagoonal patch reefs surrounded by marls	FA1
SF2.4	Lenticular shaped packages of highly discontinuous, chaotic, variable-thickness seismic reflections. Pinch out up slope	Variable (−1052 to −10 528)	0 to 90	0 to 90	Large features occurring at toe of slope, typically onlapping progradational HST.	Peri-reefal area	FA5

a) SF2.1 - Low amplitude, parallel seismic reflections commonly downlapped onto during subsequent progradational phases (Fig. 11A and B). Dip angles extracted from seismic data vary between 0° and 10° (Fig. 11c), while manually calculated dips are typically below 5° at the base of the slope (Fig. 15). These dips are interpreted as reflecting mud-dominated sediment (Fig. 12) (Kenter, 1990). Results are comparable to FA3 at Cariatiz, showing equivalent slope angles. Additionally low-amplitude parallel reflections are expected from finer sediment (Table 2) and mirror the conceptual models of Kleipool et al. (2017).

b) SF2.2 - Medium-to high-amplitude, gently inclined seismic reflections (Fig. 11A and B). Dips extracted on seismic data increase upslope from 10° to 80° (Fig. 11C), while manually calculated dips increase upslope from 5° to 30° (Fig. 15). Discrete packages exhibit sigmoid to sigmoid-oblique geometries (Fig. 11A). Reflection thickness is variable, often thickening in the upper part of the slope, a character mirrored by an increase in seismic amplitude upslope (Figs. 11A and 15). Clinoform tops were often truncated during strata progradation (Fig. 6C). These clinoforms are interpreted as mud-free, cohesionless granular facies (Figs. 11A and 12), which transition downslope to granular non-cohesive facies with minor muds (Kenter, 1990; Bachtel et al., 2004) (Figs. 12 and 15), similar to FA5 (Table 2). When compared with the outcrop data, SF2.1 correlates with FA2. Increased amplitude at the top of the slope follows the conceptual models in Kleipool et al. (2017), which propose a marked contrast in acoustic properties between reefal and lagoonal facies, both observed at Cariatiz. While the dominance of Porites corals at Cariatiz may not reflect the coral types in the Browse Basin, given the different basinal settings, results suggest they share similar characteristic and reef-framework positions. Given the heavily cemented nature of Cariatiz, the exact nature of the talus slope may vary. However, variance time slices (Fig. 13B) show that debris talus in the Browse Basin comprise large blocks on a comparable scale to SE Spain. Clinoform truncations (Figs. 6C, 11A and 11B) suggest erosion during subaerial exposure, likely resulting in a variable thickness of reef-framework facies (Fig. 12), as also documented at Cariatiz (Fig. 16).

c) SF2.3 - Variable amplitude, parallel seismic reflections (Fig. 11A and B). Attribute extracted dips are chiefly less than 10°, but locally reach 90° (Fig. 11C). Manual dip calculations record values less than 10° (Fig. 15). Where preserved, the transition between SF2.2 to SF2.3 is marked by a sharp decrease in dip (Fig. 11C). Clinoform tops are marked by the presence of low-frequency seismic components (Fig. 11D). Subtle topography is observed along seismic reflections, as also highlighted by a decrease in instantaneous frequency (Fig. 11D), as well as by the onlapping relationships of seismic reflections filling depressions. Column-like discontinuities with extracted dips of up to 90° are common within SF2.3 (Fig. 11C) and mirror the position of discontinuous seismic reflections (Fig. 11A). They form circular depressions with high variance (Fig. 13C). SF2.3 is interpreted to comprise mud-rich lagoonal and carbonate shoal facies with grain supported patch reefs comparable to FA4 (Kenter, 1990; Bachtel et al., 2004; Belde et al., 2017) (Figs. 12 and 17). We interpret a reef framework to mark the sharp decrease in dip angle between SF2.3 and SF2.2 (Figs. 11C and 12), similar to what is observed at Cariatiz. Discontinuities in seismic reflections corresponding to high-variance circular to sub-circular depressions (Fig. 11A and C) are interpreted as collapse structures of paleocave systems (Kerans, 1988; Loucks, 1999; Loucks and Mescher, 2002; McDonnell et al., 2007; Qi and Castagna, 2013; El-Eman et al., 2013; Dou et al., 2011).

d) SF2.4 - Lenticular bodies of highly discontinuous, variable amplitude, chaotic seismic reflections formed at the base of the slope, often with erosive bases (Fig. 11A). Dips estimated from seismic data range between 0° and 90° (Fig. 11C), i.e. they are equivalent to manually calculated dips (Table 2). Discrete seismic reflections

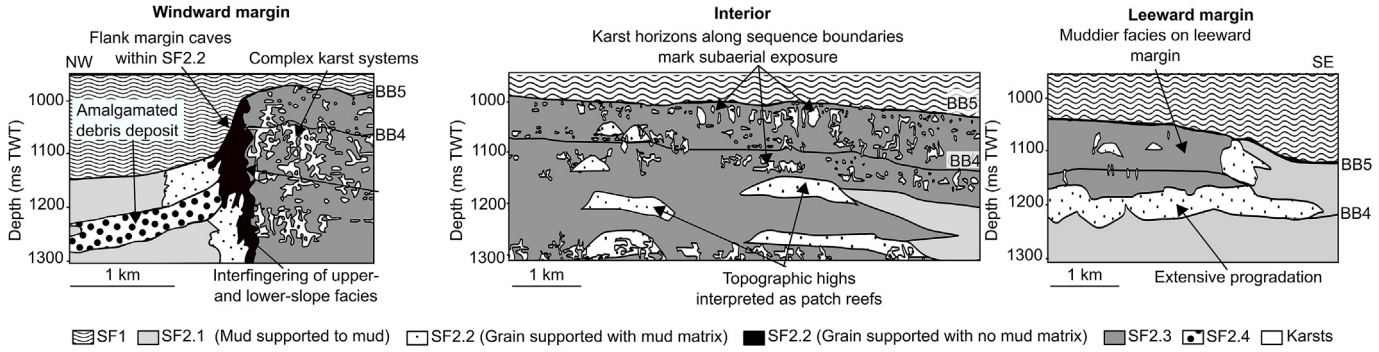

Fig. 12. Cartoon showing the interpreted facies associations based on seismic attribute analyses. Windward margins have cleaner grain-supported facies when compared to leeward margins. Windward margins are also steeper due to the relatively higher energy environment in which they form. A well-developed reef framework is interpreted at the top of slope on the windward margin, but is not clear on the leeward margin. Debrites (SF2.4) on the lower slope indicate platform shedding. Based on their size, they either represent a single episode of mass wasting, or an amalgamation of deposits shed from the build-up during its growth. The greater dips at the top of the slope (SF2.2) are thought to be attenuated by the presence of discontinuous seismic reflections, as SF2.2 can also host flank-margin caves. Build-up interiors are interpreted to comprise coarse-grained facies of patch reefs interbedded with muds and marls. Karst intervals are clearly observed along sequence boundaries and suggest sub-aerial exposure. Results show these boundaries to reflect quite extensive systems of karsts and cave systems with different ages.

show variable thickness. Lenses thin and pinch-out upslope where they onlap onto underlying strata. Instantaneous phase is highly discontinuous within this facies (Fig. 11B). SF2.4 is interpreted as comprising lowstand peri-reefal debrites similar to FA5 (Table 2 and Fig. 12). They are the result of margin collapse (Fig. 13B) due to oversteepening and shedding of sediment by gravity processes following subaerial exposure (Vail et al., 1991; Fournier et al., 2005).

7. Discussion

7.1. In what ways did eustatic sea level change and tectonics control Miocene reef growth in the Browse Basin?

The correlation between age markers from the Torosa well, and the seismic units interpreted in this paper, shows the deposition of Unit 1 to be consistent in both timing and morphology with CPP-2 of Belde et al. (2017), interpreted to the south of the study area (Fig. 18). Our results agree with Belde et al. (2017) when considering that the Browse Basin entered tropical latitudes between 17.5 Ma and 15 Ma (Aquitanian – Langhian), promoting widespread reef growth. Hence, our Unit 2 is equivalent to CPP-3 (Belde et al., 2017) and materialises reef growth constrained by the antecedent topography of clinoforms below BB1, and by variable accommodation space creation from 15 Ma to 11 Ma (see also Van Tuyl et al., 2018) (Fig. 18). In comparison, Units 3 and 4 record marked variations in the creation and loss of accommodation space, correlating with unit CPP-4 (Belde et al., 2017) and spanning 11 Ma and 4.8 Ma (Tortonian-Messinian).

The period spanning the Middle to Late Miocene is dominated by collision-driven tectonic inversion (Kennard et al., 2004; Rosleff-Soerensen et al., 2016; Belde et al., 2017). Our results found no evidence for fault-related topography created at this time in the study area, i.e. inversion anticlines (O'Brien et al., 1996; Rosleff-Soerensen et al., 2016), to influence build-up evolution in the Browse Basin (Figs. 3–5).

Faults observed in the eastern part of the study area were generated during the later stages of reef growth (Unit 3 and Unit 4) (Fig. 8B, (A and 9B), and do not influence build-up growth (Figs. 5–7). The lack of fault structures (e.g. inversion anticlines) within the interpreted seismic volume implies that pre-existing (syn- and early post-rift) faults were not reactivated by ongoing collision and subduction, which was concentrated to the north of the study area.

The appearance of these features in the southern part of the Browse Basin (Rosleff-Soerensen et al., 2016; Belde et al., 2017), but not in the study area, may be associated with regional strain partitioning as the North West Shelf migrated northwards during the Miocene (McCaffrey, 1996), as also suggested for the Barcoo sub-basin (Butcher, 1989; Haston and Williams, 1993; Symonds et al., 1994).

Rotations in the strike of underlying Jurassic and Cretaceous wrench structures (Malcom et al., 1991) likely resulted in some faults being more favourably oriented for reactivation, thus generating the different fault styles observed between the Barcoo (O'Brien et al., 1993; Rosleff-Soerensen et al., 2016; Belde et al., 2017) and Caswell sub-basins (This study; Belde et al., 2017) – a character also recorded by the Barcoo-1 and Caswell-2 wells (Kennard et al., 2004). Tectonic inversion is documented along the eastern margin of the Caswell sub-basin due to fault reactivation during the Miocene (Symonds et al., 1994). Our results, therefore, favour the postulate that collision-related stress in the Late Miocene was strongly partitioned along the North West Shelf, and that strain was concentrated around faults favourably oriented to be reactivated, e.g. the Barcoo Fault Zone in the Barcoo sub-basin and the eastern margin of the Caswell sub-basin. As a result, little to no Neogene deformation occurred away from these zones (Keep et al., 1998). This postulate also explains why we observe an easterly dip to Miocene horizons in the Browse Basin (Figs. 7–9).

A key result from this study is that build-ups were exposed between 11.1 and > 4.5 Ma (Units 3 and 4), with extensive karst intervals characterising sequence boundaries BB4 and BB5 on seismic data. Current studies propose that subsidence rates in the Browse Basin ranged from 60 m/Myr (Czarnota et al., 2013) to 125 m/Myr (Belde et al., 2017) after 15 Ma. Rosleff-Soerensen et al. (2016) suggested that accelerated subsidence rates were too large to be attenuated by the globally recognised Messinian eustatic lowstand (Haq et al., 1987; Gorini et al., 2015; Miller et al., 2005), and proposed retrogradational growth onto inversion anticlines during the Messinian.

The interpreted data show no evidence for significant retrogradation due to accelerated subsidence in the Messinian (Figs. 3–5). Thus, our results show that even if subsidence rates after 15 Ma were close to 125 m/Myr (Belde et al., 2017), the latest Miocene eustatic sea-level drop was sufficiently important to attenuate subsidence rates and generate lowstand conditions, promoting progradation and exposure in Units 3 and 4 (Figs. 3–6). Consequently, if other conditions for reef growth (e.g. light intensity, nutrients available, water quality, etc.) were favourable across the Browse Basin during the Late Miocene, the

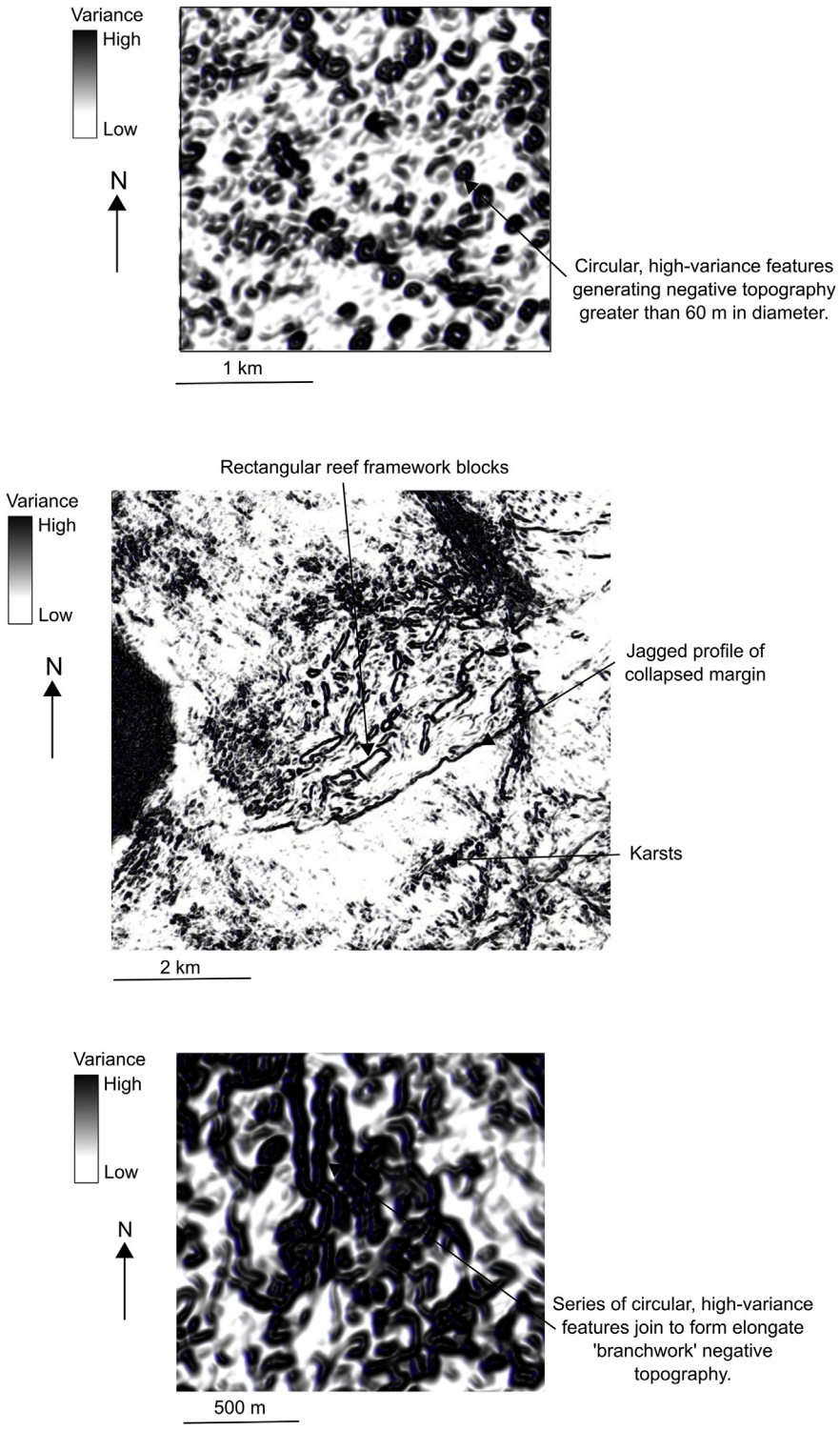

Fig. 13. (A) Variance time slice at Z = −1400 ms TWT showing circular, high-variance features correlating with discontinuities in seismic reflections and negative topography with diameters greater than 60 m. These features are interpreted as karsts and represent the collapse of smaller multi-layer karst systems. (B) Variance time slice at Z = −1750 ms TWT showing a debris talus within Unit 1 at the base of a collapsed margin. The jagged profile of the collapsed margin is clearly observed, as are slide blocks. These blocks show a dominant northeast trend and decrease in size towards the base of the slope. (C) Variance time slice at Z = −1030 ms TWT showing circular to sub-circular, high-variance features which join to form elongate 'branchwork' features with negative topography. These are interpreted as karsts, which represent dendritic drainage patterns stemming from topographic highs above discrete build-ups.

data in this paper suggest that carbonate accumulation rates were significantly larger in the northern Browse Basin, and capable of keeping carbonate build-up within the photic zone during intervals of significant accommodation creation (e.g. McNeill, 2005; Kemp et al., 2014), without the need to retrograde onto topographic highs. An alternative explanation is that subsidence rates in the Barcoo sub-basin were greater than the Caswell sub-basin, thus forcing retrogradation of carbonate build-ups onto topographic highs.

7.2. At what scale is seismic interpretation comparable with outcrop data?

Carbonate build-ups are readily differentiated from enveloping strata in the Browse Basin seismic volume (Fig. 11). The large-scale build-ups in the study area are comparable to those to the south

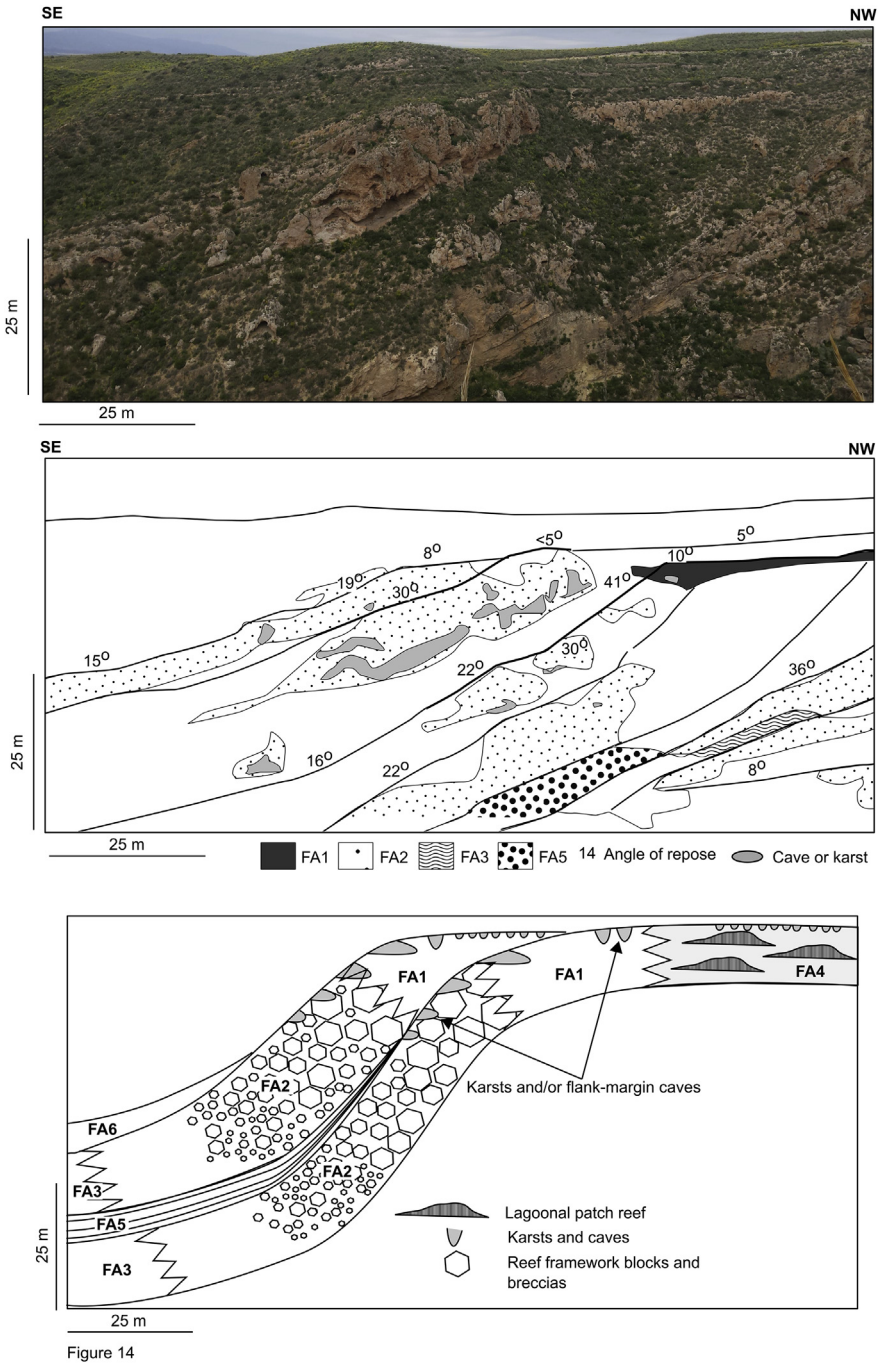

Figure 14

Fig. 14. (A) Panoramic photo looking southwest at prograding clinoforms in the Cariatiz reef. (B) Line drawing of (A) showing the geometry of clinoforms, as well as facies associations and the dips of clinoforms. Given a present-day tectonic tilt of 1.6° in the direction of progradation (Braga and Martín, 1996), clinoforms reach a maximum of 40° and show a downslope decrease in slope angle, with the platform top having a dip of 5°. (C) Cartoon showing the distribution of interpreted facies associations in the Cariatiz Reef. Lagoonal facies (FA4) comprise coarser-grained facies of patch reefs interbedded with muds and marls. Moving towards the windward margin facies transition of reef-framework Porities, which are heavily cemented (FA1). The upper slope comprised reef-framework blocks and breccias, which decrease in size downslope, where FA2 interfingers with basinal mud facies in FA3. Lower-slope facies are often interspersed with stratified coarse-grained siliciclastics sourced from the reef interior and hinterland, deposited during sea-level lowstands (FA5). Chaotic conglomeratic deposits are often associated with these lowstands and contain large clasts of reef-framework and hinterland strata (FA6). Centimetre-scale karsts are observed in lagoonal areas, particularly on topographic highs. Windward margins exhibit larger karsts with 'chimney-like' geometries. Their presence is particularly noted within FA1 and FA2.

(Rosleff-Soerensen et al., 2016; Belde et al., 2017), as well as with the Cariatiz Reef of southeast Spain (Fig. 15).

Seismic attribute analyses (Fig. 11) showed the northwest margins of the build-ups to be steeper and coarser-grained when compared to the relatively lower angle, muddier southeast margins (Fig. 12), a character agreeing with data in Bachtel et al. (2004), Belde et al. (2017), and with the Cariatiz Reef. Hence, the northwest flanks of the build-ups are interpreted as the windward margins, and the southeast flanks as leeward margins reflecting a decrease in energy moving northwest to southeast across a build-up (Fig. 12). Seismic attributes across reef margins consistently show a downslope transition from grain-supported facies at the top of the build-up margins to mud-rich facies. Furthermore, attribute analyses show that the vertical (and lateral) continuity of facies associations is clearer on the northwest (windward) margins, and more compartmentalised on southeast (leeward) margins (Fig. 11). At outcrop, a key observation is that, during lowstands, significant erosion of upper slope material can remove large amounts of the reef-framework facies (Fig. 16). This phenomenon is not clearly imaged on seismic data due to limited vertical resolution (Fig. 11). As a result, seismic reflection geometry suggests that reef-framework facies are preserved within the preceding clinoform, but this is not always the case. Upper slope erosion must be considered when

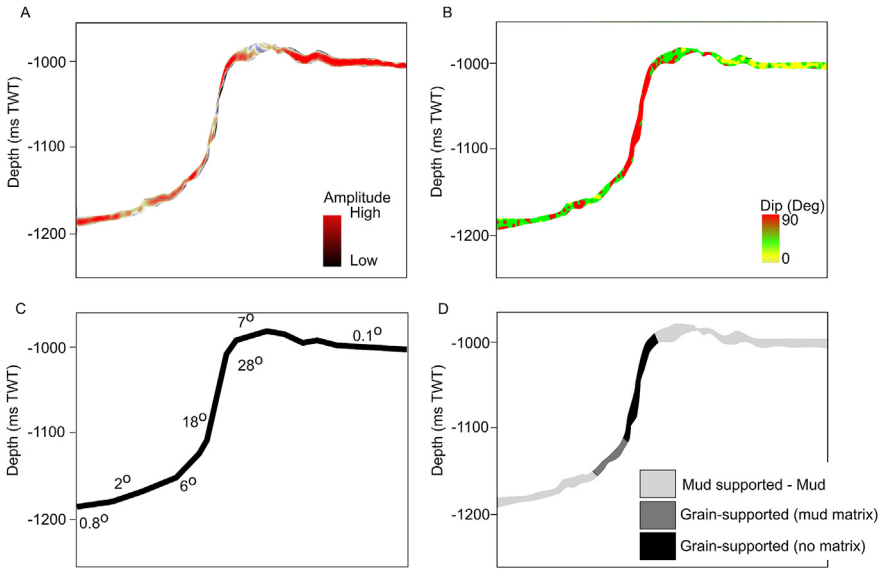

Fig. 15. Series of cross-sections of an individual seismic reflection showing the (A) seismic amplitude, (B) dip attribute, (C) manually calculated angle of repose and (D) facies interpretation. Seismic amplitude (A) is highest at the top of slope, generally decreasing downslope. Dip angle (B) increases upslope, before sharply decreasing into the low-angle build-up interior. Manually calculated angles of repose (C) for the seismic reflection mirror the results of extracted dip attributes - they show similar trends, although with slightly lower angles for the manually interpreted values. Interpretation of the seismic reflection based on angles of repose (D) shows the lagoonal area to comprise mud to mud-supported facies. The upper slope comprises grain–supported facies with no mud matrix. These transition through grain-supported facies with a mud matrix (mid slope) towards mud-supported and mud facies at the base of slope.

predicting reservoir potential in carbonate build-ups.

Debris intervals are interpreted at the base of windward margins, reflecting margin collapse and the re-deposition of material eroded from the build-ups during sea-level lowstands (Figs. 11A and 13B). Typically over 70 m thick (Fig. 11A), such deposits are indicative of discrete (but large scale) episodes of mass-wasting from the platform margin, (e.g. Principaud et al., 2015), or the stacking of smaller debrites over the life of carbonate build-ups. At Cariatiz, m-scale lowstand mass-transport deposits (FA5) are interbedded with lower-slope facies (FA2) (Braga and Martín, 1996; Reolid et al., 2016) (Fig. 16B). However, their

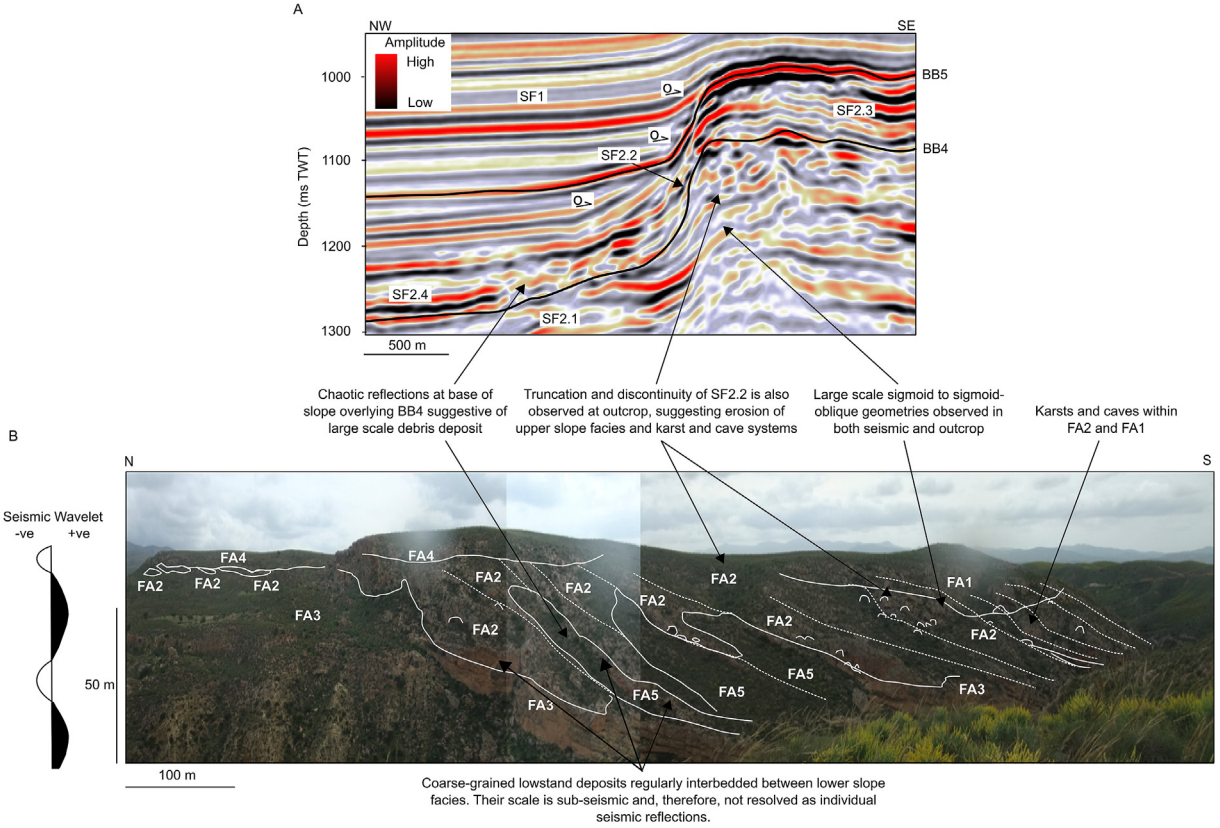

Fig. 16. Comparison of windward margin interpretations between (A) a selected seismic profile from the Poseidon 3D volume, and (B) the Cariatiz Reef outcrop. The comparison in this figure shows that while the Browse Basin seismic volume has excellent vertical and horizontal resolutions, numerous outcrop-scale features could not be imaged, or are difficult to interpret. This limitation is particularly obvious when considering lower-slope debris deposits, whose thickness is at, or below, the resolution of the interpreted seismic volume comprising a single wavelet constructively imaged with other lower-slope facies. In addition, at outcrop and seismic data are observed prominent truncations in upper-slope clinoforms. At outcrop, this results in a highly variable thickness of reef-framework facies. In some cases reef-framework facies are completely absent, and upper slope facies are directly overlain by lagoonal strata. These subtle differences are difficult to determine using seismic data while one could assume that reef-framework facies may occupy the top of the slope, this may not be the case when comparing the seismic interpretations with outcrop information.

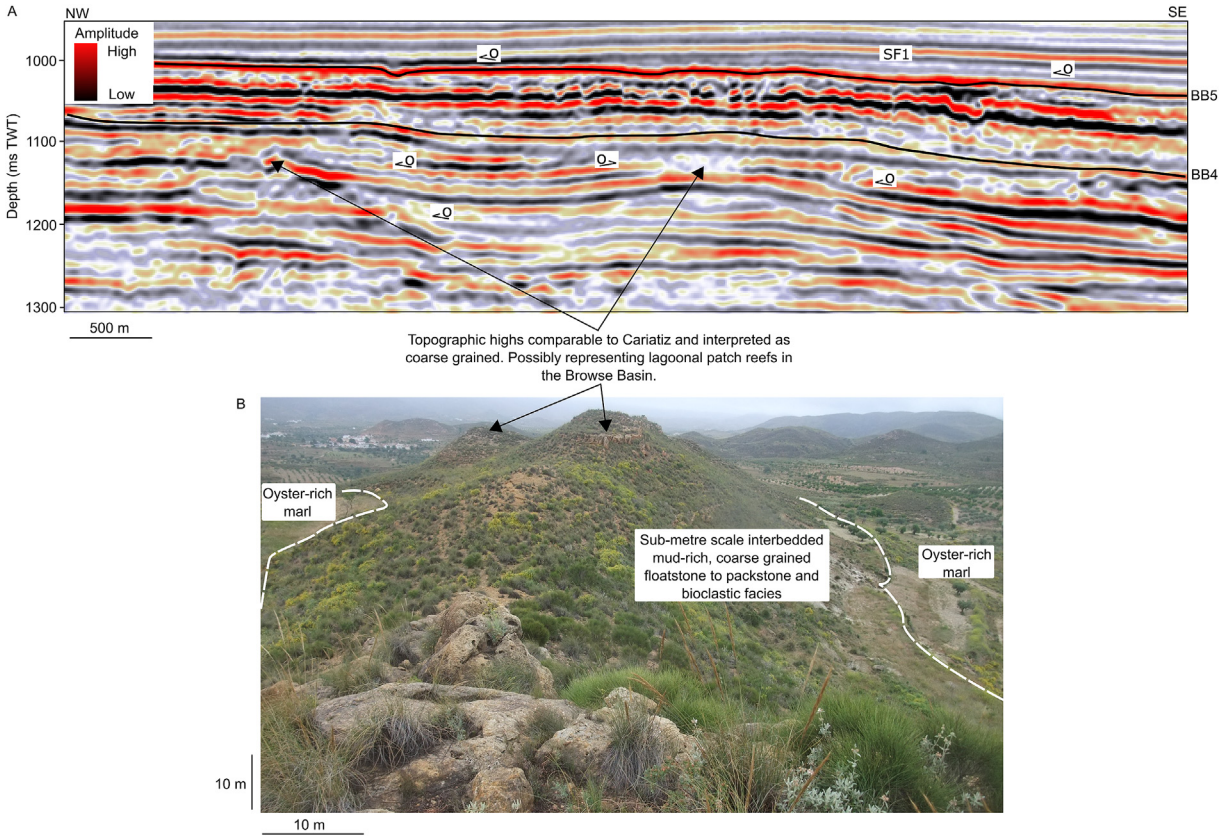

Fig. 17. (A) Seismic profile through a build-up interior. Subtle topography is observed below onlapping reflections, suggesting the presence of patch reefs and onlapping lagoonal muds and marls. (B) Photograph of the lagoonal area at Cariatiz, showing coarse-grained topographic highs onlapped by oyster-rich marls suggestive of a similar lagoonal environment.

geometries and sizes at outcrop are below the resolution of the interpreted seismic volume (Fig. 16A). Consequently, further debrites are expected to occur on the lower slope of the Browse Basin, but are not imaged by the Poseidon seismic volume. These peri-reefal deposits comprise a significant component of reservoir facies within the overall carbonate build-up. Consequently, incomplete interpretations of these features resulting from their sub-seismic scale(s) can lead to significant underestimations of reservoir potential in lower-slope areas.

Seismic attribute interpretations of the build-up interior facies proved relatively difficult (Figs. 11 and 12). Dip attribute values for discrete seismic reflections, while highly variable along karst intervals, generally showed relatively low dips – a character suggesting muddier facies (Fig. 11C). Observed topographic highs are suggestive of coarser-grain facies, with intervening depressions infilled by onlapping muddier facies, as observed in the Cariatiz Reef (Fig. 17A and B). As such, we interpret interior seismic facies to comprise isolated patch reefs, interspersed by areas of lagoonal and carbonate shoal facies (see Belde et al., 2017).

While the general trends reflected by our seismic attribute analyses mirror the interpretations from other carbonate build-ups (e.g. Kenter, 1990; Bachtel et al., 2004; Belde et al., 2017), extracted dip angles approaching 90° were observed locally along the at and inclined seismic reflections that form build-up margins and interiors (Fig. 11C). Manual dip calculations found the dips extracted from seismic data to be greatly exaggerated (Fig. 15). Near-vertical margins are documented in nature (e.g. Ginsburg et al., 1991; Phelps and Kerans, 2010) notably: a) where the reef margin is heavily cemented, b) where the reef margin had previously collapsed due to fracture networks and undercutting during lowstands (Hopley, 2006), or c) where the pre-existing topography (e.g. fault-related) prevented the development of a slope (Wilson et al., 2000). However, our results showed no definitive evidence for these three processes. Additionally, the heavily cemented Cariatiz Reef margin could only attain a maximum dip of 41° (Fig. 14A). Syn- or post-depositional tilting of build-ups due to regional tectonics (e.g. Wilson et al., 2000; Rosleff-Soerensen et al., 2016; Belde et al., 2017) appears unlikely to have caused exaggerated or attenuated dip angles as reef tops in Unit 4 are found to dip to the southeast by less than one degree (1°). Consequently, our preferred explanation is that anomalously extracted dip angles are caused by disruptions along seismic reflections, notably karstified intervals (Fig. 11). We suggest that the anomalous angles may be representative of karsts and flank-margin caves (James and Choquette, 1990; Mylroie and Carew, 1990, 1995) and not the angles of repose of the build-up margins. As such, our results show the importance of quality controlling seismic-attribute data, and that once this quality control has been undertaken, attribute analyses can comprise an effective tool for facies interpretations.

Our facies interpretation provides insight into the paleogeographic evolution of the study area through the Miocene (Figs. 7–9). In Unit 1, a northeast striking build-up, traceable to the southwest (Rosleff-Soerensen et al., 2016; Belde et al., 2017), protected an area of muds, marls, amalgamated shoals and patch reefs to the east. The initial aggradational phase of this build-up generated a thick, laterally extensive unit of reef-framework and debris-talus facies. Reef-facies in Unit 1 were eroded during the sea-level fall that promoted the karstifcation of BB2, and resulting strata were re-deposited as a thick debrites at the base of the slope (Fig. 13B). Thereafter, reef-framework and slope facies prograded onto the basin margin, restricted by the antecedent topography (Belde et al., 2017) (Figs. 7B and 8A). Debrites mark the base of the slope, and the barrier build-up was backed by a protected lagoonal area of muds, marls, patch reefs and carbonate shoals. This margin build-up is imaged to the south (Belde et al., 2017) and suggests it formed a basin-wide feature.

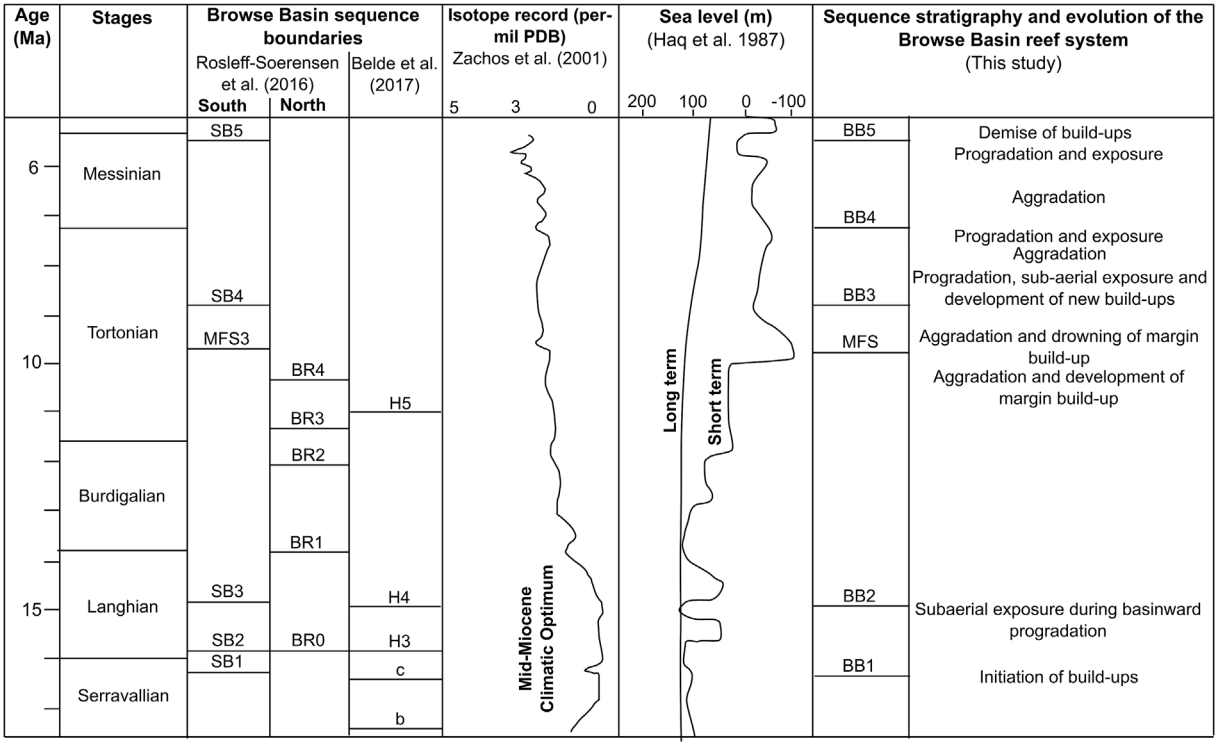

Fig. 18. Summary of the interpreted evolution and timing of sequence boundaries in the study area compared to published data on the Browse Basin. The sequence boundaries BB1 and BB2 show a good correlation with Belde et al. (2017) and sea-level curves in Haq et al. (1987). Thereafter, correlation becomes difficult. However, BB3 and BB4 are definitely younger than 10 Ma and older than 4.8 Ma. The rapid aggradation interpreted in Unit 2 is observed across the North West Shelf, and, therefore, MFS 2 is suggested to be around 9.5 Ma (Rosleff-Soerensen, 2012). Growth patterns during Units 3 and 4 correlate with a Messinian lowstand suggested by oxygen isotope records (Zachos et al., 2001) and sea-level curves (Haq et al., 1987; Miller et al., 2005). During the Messinian lowstand, small-scale sea-level changes facilitated the accumulation of alternating aggradational and progradational strata.

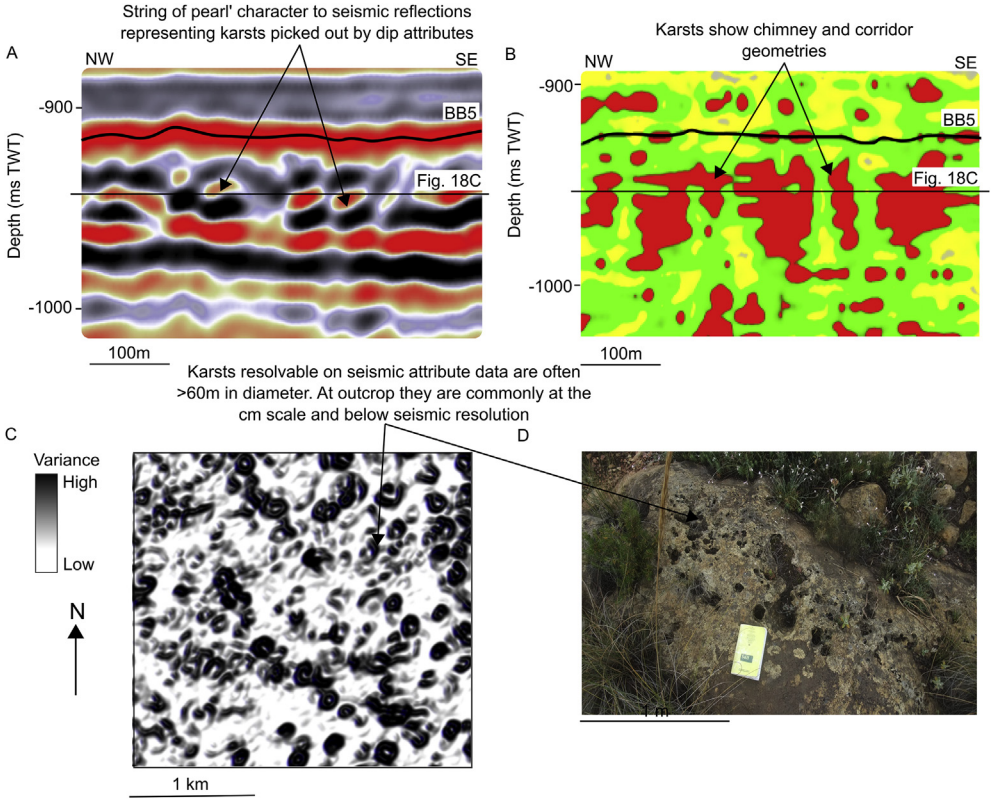

Fig. 19. (A) Seismic line showing the 'string of pearl' character of strata with developed karsts. (B) Dip attribute profile highlighting karsts as forming 'chimney-like' features with high dip angles. (C) Variance time-slice at Z = −1400 ms TWT showing dendritic karst patterns. Karsts are in excess of 60 m in diameter and are interpreted as collapse structures linking different karst networks. Comparison to centimetre scale karsts at outcrop (D) shows that karsts resolved on seismic data comprise only the largest features. Consequently, karst frequency is likely to be significantly higher than that interpreted from seismic data alone.

The aggradational phase recorded in Unit 2 buried the carbonate build-ups under muddier facies (SF1) (Fig. 8B). Drowning of the barrier build-up established open-water conditions in the southeast of the study area, with isolated build-up morphologies reflecting an increase in energy by developing steeper northwest, northern, and northeast margins. This change in conditions is also demonstrated in the northern part of the study area where leeward-margin facies are observed to rotate from northwest to west (8B, 9A, and 9B). Such a change possibly reflects variations in the orientation of the prevailing wind and current directions as the North West Shelf migrated north and rotated during the Miocene in response to subduction in the Timor Trough (Keep et al., 1998). The appearance of numerous intra-platform seaways oriented perpendicularly to the interpreted wind and current directions during Units 3 and 4 suggest that localised currents influenced build-morphology, as reflected by the steepening and shaping of the build-up margins that border intra-platform seaways.

7.3. Seismic attribute analyses as a competent method to characterise karst systems

Within build-up interiors, seismic attributes proved very effective in imaging dendritic karst networks at sequence boundaries (Figs. 13C and 19), as also documented in southeast Asia (Vahrenkamp et al., 2004; Fournillon et al., 2012; Jacquemyn et al., 2012; Zhao et al., 2014). The increased pervasiveness of karsts above topographic highs in build-up interiors (Fig. 17A) concurs with observations from the Cariatiz Reef (Fig. 17B), as well as from the Tamrin Basin (Zhang and Liu., 2009; Zhao et al., 2014), with prolonged subaerial exposure during relative sea-level lowstands extending denudation and promoting extensive epigenetic dissolution of the reef interior by meteoric fluids (Wright et al., 2014). Seismic attributes also recognise discontinuities in seismic reflections as correlating with high-angle columns (crossing seismic reflections) that are connected by horizontal corridors parallel to seismic reflections (Figs. 11C and 19). The geometry of these karsts, their position on windward margins, added to the observation that they do not typically correspond to sequence boundaries, is not only similar to the Cariatiz Reef; it also suggests the presence of hypogenic flank-margin and phreatic caves documented on other carbonate islands and land-attached carbonate platforms (James and Choquette, 1990; Mylroie and Carew, 1990, 1995).

It must be taken into account, however, that karsts identified by seismic attributes are typically over 60 m in diameter in the Browse Basin and do not compare directly to karsts and caves observed at outcrop, which are commonly cm to m scale (Fig. 19). This latter fact suggests that karsts resolved by the interpreted seismic volume are representative of the collapse of multi-layer karst and cave systems (Qi et al., 2013), e.g. dolines (Waltham and Fookes, 2003) similar to those documented in Slovenia (Gospodaric, 1985), China (Waltham et al., 1993), eastern Brazil (Bastos et al., 2016), and the Yucatan Peninsula, Mexico (Stringfield and LeGrand, 1976).

The results of our study show that seismic interpretation and attribute analyses are effective tools for delineating facies associations and karsts within carbonate build-ups. However, our results also show that the quality of one's interpretation also depends on seismic resolution. Comparison between the scale of features interpreted from a seismic volume and their outcrop counterparts highlighted the limitation that seismic resolution imparts in terms of not imaging karsts below threshold vertical and horizontal resolutions. This limitation may have a significant impact on hydrocarbon production strategies, such as elevated production tests representative of karsts rather than the host formation, mud-circulation losses and drill-bit drops (Zhao et al., 2014). Consequently, our results confirm the importance of considering seismic resolution in the interpretation of carbonate build-ups, as well as employing appropriate outcrop analogues in reservoir characterisation.

8. Conclusions

Based on the interpretation of the Browse Basin seismic volume, in the context of the regional evolution of the North West Shelf during the Miocene, this work reached the following conclusions:

1. Five sequence boundaries are identified within the Miocene tropical carbonate sequence of the Browse Basin. They reveal two sea level lowstands (Langhian and Messinian), interspersed by a major aggradational phase during the Tortonian.
2. Five seismic facies were identified (SF1, SF2.1 to SF2.4). Based on seismic analyses and outcrop data, we document an upslope transition from lower slope muds through a talus slope into the reef framework and lagoon.
3. The Browse Basin experienced structural partitioning during the Messinian, which saw faulting and processes associated with plate collision (e.g. inversion) restricted to preferentially oriented faults, notably in the Barcoo Sub Basin and the eastern Caswell sub-basin, with little tectonic influence felt away from these zones. Thus fault tectonics are thought to affect Miocene carbonate build-ups only locally and, therefore, eustatic sea-level was the primary control on platform evolution in the study area.
4. Seismic attribute analyses proved a highly effective tool for interpreting carbonate facies. However, they are limited to large-scale features and facies belts, i.e. they do not image features at the scales observed in the field (Cariatiz Reef, southeast Spain). Consequently, estimations of reservoir potential are likely to be significantly underestimated if based on seismic data alone.

Acknowledgments

We thank the support of the NERC Centre of Doctoral Training in Oil and Gas (NERC Oil and Gas CDT Grant NE/M00578X/1), which was co-sponsored by Cardiff University. Schlumberger provided (Petrel) academic licenses to Cardiff. This work used data from Geosciences Australia, whom we duly acknowledge.

References

Ahr, W.M., 2008. Geology of Carbonate Reservoirs: the Identification, Description and Characterization of Hydrocarbon Reservoirs in Carbonate Rocks. Wiley, pp. 265.
Anselmetti, F., Eberli, G.P., Ding, Z.-D., 2000. From the Great Bahama Bank into the Straits of Florida: a margin architecture controlled by sea-level fluctuations and ocean currents. Geol. Soc. Am. Bull. 112, 829–844.
Apthorpe, M., 1988. Cainozoic depositional history of the North West shelf. In: Purcell, P.G., Purcell, R.R. (Eds.), Proceedings of Petroleum Exploration Society of Western Australia Symposium, Perth. The North West Shelf, Australia, pp. 55–84.
Bachtel, S.L., Kissling, R.D., Martono, D., Rhardjanto, S.P., Dunn, P.A., MacDonald, B.A., 2004. Seismic stratigraphic evolution of the Miocene-Pliocene Segitiga Platform, East Natuna Sea, Indonesia: the origin, growth, and demise of an isolated carbonate platform. In: Seismic Imaging of Carbonate Reservoirs and Systems, vol. 81. AAPG Memoir, pp. 309–328.
Baille, P.W., Powell, C., Me, A., Li, Z.X., Ryall, A.M., 1994. The tectonic framework of western Australia's Neoproterozoic to Recent sedimentary basins. In: Purcell, P.G., Purcell, R.R. (Eds.), The Sedimentary Basins of Western Australia: Proceedings of Petroleum Exploration Society of Australia, Symposium, Perth 1994, pp. 45–62.
Bastos, A.C., Amado-Filho, G.M., Moura, R.L., Braga, J.C., Sampaio, F.M., Bassi, D., 2016. Origin and sedimentary evolution of sinkholes (buracas) in the Abrolhos continental shelf, Brazil. Palaeogeogr. Palaeoclimatol. Palaeoecol. 462, 101–111.
Belde, J., Back, S., Bourget, J., Reuning, L., 2017. Oligocene and Miocene carbonate platform development in the Browse Basin, Australian northwest shelf. J. Sediment. Res. 87, 795–816.
Blevin, J.E., Struckmeyer, H.I.M., Cathro, D.L., Totterdell, J.M., Boreham, G.J., Romine, K.K., Loutit, T.S., Sayers, J., 1998. Tectonostratigraphic framework and petroleum systems of the Browse Basin, North West Shelf. In: Purcell, P.G., Purcell, R.R. (Eds.), The Sedimentary Basins of Western Australia 2: Proceedings of the Western Australia Basins Symposium, Perth, 1998, pp. 369–396.
Bourillot, R., Vennin, E., Rouchy, J.-M., Blanc-Valleron, M.-M., Caruso, A., Durlet, C., 2010. The end of the Messinian Salinity Crisis in the western Mediterranean: insights from the carbonate platforms of south-eastern Spain. Sediment. Geol. 229, 224–253.
Bradshaw, M.T., Bradshaw, J., Murray, A., Needham, J., Spencer, L., Summons, R.E., Wilmot, J., Winn, S., 1994. Petroleum systems in west Australian basins. In: Purcell, P.G., Purcell, R.R. (Eds.), The Sedimentary Basins of Western Australia: Proceedings of the Petroleum Exploration Society of Australia, Perth, 1994, pp. 93–118.

Braga, J.C., Martín, J.M., 1996. Geometries of reef advance in response to relative sea-level changes in a Messinian (uppermost Miocene) fringing reef (Cariatiz Reef, Sorbas Basin, SE Spain). Sediment. Geol. 107, 61–81.
Butcher, B.P., 1989. Northwest shelf, Australia. In: Edwards, J.D., Santagrossi, P.A. (Eds.), Divergent/passive Margins. American Association of Petroleum Geologists, pp. 81–116.
Chang, J.H., Hsu, H.H., Lee, T.Y., Chiu, S.D., Su, C.C., Ma, Y.F., Chiu, Y.H., Hung, H.T., Lin, Y.C., Chiu, C.H., 2017. Seismic sequence stratigraphic analysis of the carbonate platform, north offshore Taiping Island, Dangerous Grounds, South China Sea. Tectonophysics. https://doi.org/10.1016/j.tecto.2015.12.010.
ConocoPhillips, 2011a. Poseidon-1 Well Completion Report, vol. 2. pp. 1–44 Interpretive Data.
ConocoPhillips, 2011b. Kronos-1 Well Completion Report, vol. 2. pp. 1–954 Interpretive Data.
ConocoPhillips, 2012. WA-315-P and WA398-P Browse Basin Western Australia 2009 Poseidon 3D Marine Surface Seismic Survey. Interpretation Report. pp. 1–43.
Czarnota, K., Hoggard, M.J., White, N., Winterbourne, J., 2013. Spatial and temporal patterns of Cenozoic dynamic topography around Australia. G-cubed 14, 634–658.
Dou, Q., Sun, Y., Sullivan, C., Guo, H., 2011. Paleokarst system development in the San Andres formation, Permian basin, revealed by seismic characterization. J. Appl. Geophys. 75, 379–389. https://doi.org/10.1016/j.jappgeo.2011.08.003.
Dunham, R.J., 1962. Classification of carbonate rocks according to depositional texture. In: Ham, W.E. (Ed.), Classification of Carbonate Rocks. American Association of Petroleum Geologists Memoir, pp. 108–121.
Ehrenberg, S.N., Nadeau, P.H., Aqrawi, A.A.M., 2007. AAPG Bull. 91 (3), 275–286.
El-Eman, A., Ebaid, A., Zahran, W., Al-Ajmi, B., Kuwait, Oil Company, Saleh, T., Cunnell, C., Laake, A., El Din, R.S., Wahab, H.A., WesternGeco, 2013. Delineation of karsts, a new approach using seismic attributes – case study from Kuwait. In: SEG Houston 2013 Annual Meeting, pp. 3846–3850.
Erlich, R.N., Barrett, S.F., Ju, G.B., 1990. Seismic and geological characteristics of drowning event on carbonate platforms. AAPG Bull. 74 (10), 1523–1537.
Fournier, F., Borgomano, J., Motaggioni, L.F., 2005. Development patterns and controlling factors of Tertiary carbonate build-ups: insights from high-resolution 3D seismic and well data in the Malampaya gas field (Offshore Palawan, Philippines). Sediment. Geol. 175, 189–215.
Fournillon, A., Aberlard, S., Viseur, R., Ar b, B., Borgomano, J., 2012. Characterization of karstic networks by automatic extraction of geometrical and topological parameters: comparison between observations and stochastic simulations. In: In: Garland, J., Neilson, J.E., Laubach, S.E., Whidden, K.J. (Eds.), Advances in Carbonate Exploration and Reservoir Analysis, vol. 370. Geological Society, London, pp. 247–264 (Special Publications).
Ginsburg, R.N., Harris, P.M., Eberli, G.P., Swart, P.K., 1991. The growth potential of a bypass margin, Great Bahama Bank. J. Sediment. Geol. 61 (6), 976–987.
Gorini, C., Montader, L., Rabineau, M., 2015. New imaging of the salinity crisis: dual Messinian lowstand megasequences recorded in the deep basin of both the eastern and western Mediterranean. Mar. Petrol. Geol. 66, 278–294.
Gospodaric, R., 1985. The examples of classical karst of Slovenia (NW Yugoslavia) Annales de la societe Geologique de Belgique, T.. Age and Development of Collapse Dolines above the Cave Systems, vol. 108. pp. 113–116.
Gradstein, F.M., O, J.M., Schmitz, M.D., Ogg, G.M., 2012. The Geological Time Scale 2012. Elsevier, Oxford, UK, pp. 1144.
Handford, C.R., Loucks, R.G., 1993. Carbonate depositional sequences and systems tract – responses of carbonate platforms to relative sea-level changes. In: In: Loucks, R.G., Sarg, J.F. (Eds.), Carbonate Sequence Stratigraphy, vol. 57. American Association of Petroleum Geologists Memoirs, pp. 3–42.
Haq, B.U., Hardenbol, J., Vail, P.R., 1987. Chronology of fluctuation sea levels since the Triassic. Science 235, 1156–1167.
Haq, B.U., Al-Qahtani, M., 2005. Phanerozoic cycles of sea-level change on the Arabian Platform. GeoArabia 10, 127–160.
Harris, P.M., Frost, S.H., 1984. Middle cretaceous carbonate reservoirs, Fahud field and northwestern Oman. AAPG Bull. 68 (5), 649–658.
Harrowfield, M., Keep, M., 2005. Tectonic modification of the Australian North-West Shelf: episodic rejuvenation of long-lived basin divisions. Basin Res. 17 (2), 225–239.
Haston, R.B., Williams, A.F., 1993. The stress field of the North West Shelf and wellbore stability. APEA J. 33 (1), 373–385.
Ho, S., Cartwright, J.A., Imbert, P., 2012. Vertical evolution of fluid venting structures in relation to gas flux, in the Neogene-Quaternary of the Lower Congo Basin, Offshore Angola. Mar. Geol. 332–334, 40–55.
Hopley, D., 2006. Coral reef growth on the shelf margin of the Great Barrier Reef with special reference to the pompey complex. J. Coast Res. 22, 150–158.
Howarth, V., Alves, T.M., 2016. Fluid flow through carbonate platforms as evidence for deep-seated reservoirs in North West Australia. Mar. Geol. 380, 128.
Hull, J.N.F., Griffiths, C.M., 2002. Sequence Stratigraphic Evolution of the Albian to Recent Section of the Dampier Sub-basin. North West Shelf Australia. pp. 617–639.
Jacquemyn, C., Swennen, R., Ronchi, P., 2012. Mechanical stratigraphy and (palaeo-) karstification of the murge area (Apulia, southern Italy). In: In: Garland, J., Neilson, J.E., Laubach, S.E., Whidden, K.J. (Eds.), Advances in Carbonate Exploration and Reservoir Analysis, vol. 370. Geological Society, London, pp. 169–186 (Special Publications).
James, N.P., Choquette, P.W., 1990. Limestones — the meteoric diagenetic environment. In: In: Mcllreath, I.A., Morrow, D.W. (Eds.), Diagenesis: Geoscience Canada, vol. 4. pp. 35–73 (Reprint Series).
Kaiko, A.R., Tait, A.M., 2001. Post-rift tectonic subsidence and paleo-water depth in the northern Carnarvon basin, western Australia. APPEA J 41, 367–380.
Keall, J.M., Smith, P.J., 2004. The Argus-1 gas discovery, northern Browse basin, Australia. In: In: Ellis, G.K., Baillie, P.W., Munson, T.J. (Eds.), Timor Sea Petroleum Geoscience. Proceedings of the Timor Sea Symposium, Darwin, 19–20 June 2003, vol. 1. Northern Territory Geological Survey, pp. 38–52 Special Publication 2004.
Keep, M., Bishop, A., Longley, I., 2000. Neogene wrench reactivation of the Barcoo sub basin, North West Australia: implications for Neogene tectonics of the northern Australian margin. Petrol. Geosci. 6, 211–220.
Keep, M., Powell, C.McA., Baille, P.W., 1998. Neogene deformation of the North West shelf, Australia. In: Proceedings of the Sedimentary Basins of Western Australia, vol. 2. pp. 81–91.
Kemp, D.B., Sadler, P.M., Della Porta, G., 2014. Climatic and eustatic signals in a global compilation of shallow marine carbonate accumulation rates. Sedimentology 61, 1286–1297.
Kennard, J.M., Deighton, I., Ryan, D., Edwards, D.S., Boreham, C.J., 2004. Subsidence and thermal history modelling: new insights into hydrocarbon expulsion from multiple petroleum systems in the Browse Basin. In: Timor Sea Petroleum Geoscience. In: Proceedings of the Timor Sea Symposium, pp. 19–20.
Kenter, J.A.M., 1990. Carbonate platform flanks: slope angle and sediment fabric. Sedimentology 37, 777–794.
Kerans, C., 1988. Karst-controlled reservoir heterogeneity in Ellenburger Group carbonates of west Texas. AAPG Bull. 72, 1160–1183.
Kleipool, L.M., De Jong, K., De Vaal, E., Reigmer, J.J.G., 2017. Seismic characterization of switching platform geometries and dominant carbonate producers (Miocene, Las Negras, Spain). Sedimentology 64 (6), 1676–1707.
Koson, S., Piyaphong, C., Choowong, M., 2014. Seismic Attributes and Seismic Geomorphology. pp. 1–9 vol. 6(1).
Kusumastuti, A., Van Rensbergen, P.V., Warren, J.K., 2002. Seismic sequence analysis and reservoir potential of drowned Miocene carbonate platforms in the Madura Strait, East Java, Indonesia. AAPG Bull. 86 (2), 213–232.
Langhi, L., Borel, G.D., 2007. Reverse structures in accommodation zone and early compartmentalization of extension system, Laminaria High (NW shelf, Australia). Mar. Petrol. Geol. 25, 791–803.
Longley, I.M., Buessenschuett, C., Clydsdale, L., Cubitt, C.J., Davis, R.C., Johnson, M.K., Marshall, N.M., Murray, A.P., Somerville, R., Spry, T.B., Thompson, N.B., 2002. The North West shelf of Australia- a woodside perspective. In: Purcell, P.G., Purcell, R.R. (Eds.), The Sedimentary Basins of Western Australia: Proceedings of the Petroleum Exploration Society of Australia 3. Perth, 2002, pp. 27–88.
Loucks, R.G., 1999. Paleocave carbonate reservoirs: origins, burial depth modifications, spatial complexity and reservoir implications. AAPG Bull. 83, 1795–1834. http://dx.doi.org/10.1306/E4FD426F-1732-11D7-8645000102C1865D.
Loucks, R.G., Mescher, P., 2002. Coalesced-collapsed paleocave systems: origins, spatial complexity, and reservoir implications. In: Presented at AAPG Annual Meeting. Society for Sedimentary Geology Field Trip Guidebook.
Malcom, R.J., Pott, M.C., Delfos, E., 1991. A new tectonostratigraphic synthesis of the North West Cape area. APEA J. 31 (1), 154–176.
Marfurt, K.J., Alves, T.M., 2015. Pitfalls and limitations in seismic attribute interpretation of tectonic features. Interpretation 3 (1), 5–15 (February 2015).
Martín, J.M., Braga, J.C., 1994. Messinian events in the Sorbas Basin in southeastern Spain and their implications in the recent history of the Mediterranean. Sediment. Geol. 90, 257–268.
McDonnell, A., Loucks, R.G., Dooley, T., 2007. Quantifying the origin and geometry of circular sag structures in northern Fort Worth Basin, Texas: paleocave collapse, pull-apart fault systems, or hydrothermal alteration? AAPG Bull. 91, 1295–1318. http://dx.doi.org/10.1306/05170706086.
McCaffrey, R., 1996. Slip partitioning at convergent plate boundaries of SE Asia. In: In: In: Hall, R., Blundell, D. (Eds.), Tectonic Evolution of SE Asia, vol. 106. pp. 3–18 Geological Society Special Publication.
McNeill, D.F., 2005. Accumulation rates from well-dated late Neogene carbonate platforms and margins. Sediment. Geol. 175, 73–87.
Miller, K.G., Komiz, M.A., Browning, J.V., Wright, J.D., Mountain, G.S., Katz, M.E., Sugarman, P.J., Crammer, B.S., Christi-Blick, N., Pekar, S.F., 2005. The phanerozoic record of global sea-level change. Science 310, 1293–1298.
Mutti, M., Hallock, P., 2003. Carbonate systems along nutrient and temperature gradients: some sedimentological and geochemical constraints. Int. J. Earth Sci. 92, 465–475. https://doi.org/10.1007/s00531-003-0350-y.
Mylroie, J.E., Carew, J.L., 1990. Flank margin model for dissolution cave development in carbonate platforms. Earth Surf. Process. Landforms 15, 413–424. http://dx.doi.org/10.1002/esp.3290150505.
Mylroie, J.E., Carew, J.L., 1995. Karst development on carbonate islands. In: In: Budd, D.A., Saller, A.H., Harris, P.M. (Eds.), Unconformities and Porosity in Carbonate Strata, vol. 63. AAPG Memoir, pp. 55–76.
Neuhaus, D., Borgomano, J., Jauffred, J.-C., Mercadier, C., Olotu, S., Grtsch, J., 2004. Quantitative seismic reservoir characterization of an Oligocene Miocene carbonate buildup: Malampaya field, Philippines. AAPG Memoir 81, 169–183.
O'Brien, G.W., Sturrock, S., Barber, P., 1996. Vulcan tertiary tie (VTT) basin study, vulcan sub-basin, Timor Sea, northwestern Australia. In: Australian Geological Survey Organisation Record, 1996/61.
O'Brien, G.W., Etheridge, M.M.A., Willcox, J.B., Morse, M., Symonds, P., Norman, C., Needham, D.J., 1993. The structural architecture of the Timor Sea, north-western Australia: implications for basin development and hydrocarbon exploration. APEA J. 33 (1), 178–258.
Omosanya, K.O., Alves, T.M., 2013. A 3-dimensional seismic method to assess the provenance of Mass-Transport Deposits (MTDs) on salt-rich continental slopes (Espirito Santo Basin, SE Brazil). Mar. Petrol. Geol. 44, 223–239.
Phelps, R.M., Kerans, Charles, 2010. Facies and architectural variability of the Albian Stuart city margin; #90104(2010). In: AAPG National Conv. Abs.
Posamentier, H.W., Jervey, M.T., Vail, P.R., 1988. In: In: Wilgus, C.K., Hastings, B.S., Posamentier, H., Van Wagoner, J., Kendall, C.G.S.C. (Eds.), Eustatic Controls on

Clastic Deposition I – Conceptual Framework, Sea-level Changes: an Integrated Approach, vol. 42. pp. 109–124 SEPM Special Publications.
Principaud, M., Mulder, T., Gillet, H., Borgomano, J., 2015. Large-scale carbonate submarine mass wasting along the northwestern slope of the Great Bahama Bank (Bahamas). Morphology, architecture, and mechanism. Sediment. Geol. 317, 27–42.
Qi, J., Castagna, J.P., 2013. Application of a PCA fault attribute and spectral decomposition in Barnett shale fault detection. In: 83rd Annual International Meeting. SEG, pp. 1421–1425 (Expanded Abstracts).
Qi, J., Zhang, Bo, Zhou, H., Marfurt, K., 2013. Attribute expression of fault-controlled karsts, Fort Worth Basin, Texas: a tutorial. Interpretation 2 (3), 91–110.
Reolid, J., Betzler, C., Braga, J.C., 2016. Amplitude of late Miocene sea-level fluctuations from karst development in reef-slope deposits (SE Spain). Sediment. Geol. 354, 145–153.
Riding, R., Martín, J.M., Braga, J.C., 1991. Coral-stromatolite reef framework, upper Miocene, Almerfa, Spain. Sedimentology 38, 799–818.
Rosleff-Soerensen, B., Reuning, L., Back, S., Kukla, P., 2012. Seismic geomorphology and growth architecture of a Miocene barrier reef, Browse Basin, NW-Australia. Mar. Petrol. Geol. 29, 233–254.
Rosleff-Soerensen, B., Reuning, L., Back, S., Kukla, P., 2016. The response of a basin scale Miocene barrier reef system to long-term, strong subsidence on a passive continental margin, Barcoo sub-basin. Aust. North West Shelf. Basin Res. 28, 103–123.
Ruegg, G.J.H., 1964. Geologische Onderzoekingen in Het Bekken Van Sorbas. ZSpanje. Amsterdam Geological Institute, University of Amsterdam, pp. 64.
Sanchez-Almazo, I.M., Braga, J.C., Dinarès-Turell, J., Martín, J.M., Spiro, B., 2007. Palaeoceanographic controls on reef deposition: the messinian Cariatiz reef (Sorbas basin, Almería, SE Spain). Sedimentology 54 (1), 637–660.
Saqab, M.M., Bourget, J., 2015. Controls on the distribution and growth of isolated carbonate build-ups in the Timor Sea (NW Australia) during the quaternary. Mar. Petrol. Geol. 62, 123–143.
Schlager, W., 1992. Sedimentology and Sequence Stratigraphy of Reefs and Carbonate Platforms. American Association of Petroleum Geologists Continuing Education Course Note Series, Iss. 34. pp. 71.
Schlager, W., 2005. Carbonate sedimentology and sequence stratigraphy. In: SEPM Concepts in Sedimentology and Palaeontology Series No. 8, pp. 200.
Stephenson, A.E., Cadman, S.J., 1994. Browse Basin, North West Australia: the evolution, paleogeography and petroleum potential of a passive continental margin. Palaeogeogr. Palaeoclimatol. Palaeoecol. 111, 337–366.
Stringfield, V.T., LeGrand, H.E., 1976. Karst hydrology of northern Yucutan Peninsula, Mexico. In: Carbonate Rocks and Hydrogeology of the Yucatan Peninsula, Mexico, May, vols. 24–26. pp. 192–210.
Struckmeyer, H.I.M., Blevin, J.E., Sayers, J., Totterdell, J.M., Baxter, K., Cathro, D.L., 1998. Structural evolution of the Browse Basin, North West Shelf: new concepts from deep-seismic data. In: In: Purcell, P.G., Purcell, R.R. (Eds.), The Sedimentary Basins of Western Australia 2: Proceedings of the Petroleum Exploration Society of Australia Symposium, vol. 1998. pp. 345–367 (Perth, WA).
Symonds, P.A., Collins, C.D.N., Bradshaw, J., 1994. Deep structure of the Browse Basin: implications for basin development and petroleum exploration. In: Purcell, P.G., Purcell, R.R. (Eds.), The Sedimentary Basins of Western Australia: Proceedings of the Petroleum Exploration Society of Australia, Perth, 1994, pp. 315–332.
Tesch, P., Reece, R.S., Pope, M.C., Markello, J.R., 2018. Quantification of architectural variability and controls in an upper Oligocene to lower Miocene carbonate ramp, Browse Basin, Australia. Mar. Petrol. Geol. 91, 432–454.
Vahrenkamp, V.C., David, F., Duijndam, P., Crevello, P., 2004. Growth architecture, faulting, and karstification of a middle Miocene carbonate platform, Luconia province, offshore sarawak, Malaysia. In: seismic imaging of carbonate reservoirs and systems. AAPG Memoir 81, 329–350.
Vail, P.R., Audemard E Bowman, S.A., Eisner, P.N., Perez-Cruz, C., 1991. The stratigraphic signature of tectonics, eustasy and sedimentology – an overview. In: Einsele, G., Ricken, W., Seilacher, A. (Eds.), Cycles and Events in Stratigraphy. Springer-Verlag, Berlin, pp. 617–659.
Van Tuyl, J., Alves, T., Cherns, L., 2018. Pinnacle features at the base of isolated carbonate build-ups marking point-sources of fluid offshore Northwest Australia. GSA Bulletin (in press).
Van Wagoner, J.C., Posamentier, H.W., Mitchum, R.M., Vail, P.R., Sarg, J.F., Loutit, T.S., Hardenbol, J., 1988. An overview of the fundamentals of sequence stratigraphy and key definitions. In: In: Wilgus, C.K., Hastings, B.S., Kendall, C.G.S.C., Posamentier, H.W., Ross, C.A., Van Wagoner, J.C. (Eds.), Sea-level Changes: an Integrated Approach, vol. 42. pp. 39–45 SEPMM Special Publications.
Veevers, J.J., Powell, C.McA., 1984. Dextral shear within the eastern Indo-Australian plate. In: Veevers, J.J. (Ed.), Phanerozoic Earth History of Australia. Claredon Press, Oxford, pp. 102–103.
Veevers, J.J., Cotteril, D., 1978. Western margin of Australia: evolution of a rifted arch system. GSA Bulletin 89, 337–355.
Waltham, A.C., Fookes, P.G., 2003. Engineering classification of karst ground conditions. Geotech. Eng. 36, 101–118. http://dx.doi.org/10.1144/1470-9236/2002-33.
Waltham, T., Brook, D., Bottrell, S., 1993. The caves and karsts of Xigwen, China. Br. Cave Res. Assoc. 20 (3), 75–86.
Wilson, M.E., Wilson, J., Bosence, D.W.J., Limbong, A., 2000. Tertiary syntectonic carbonate platform development in Indonesia. Sedimentology 47, 395–419.
Wright, P.V., Baceta, J.I., Lapointe, P.A., 2014. Paleokarstic macroporosity development at platform margins: lessons from the Paleocene of north Spain. Interpretation 2 (3), 1–16 (August 2014).
Zachos, J., Pagani, M., Sloan, L., Thomas, E., Billups, K., 2001. Trends, rhythms, and aberrations in global climate 65 Ma to present. Science 292, 686–693.
Zampetti, V., Schlager, W., Van Konijnenburg, J.H., Everts, A.J., 2004. Architecture and growth history of a Miocene carbonate platform from 3D seismic reflection data: Luconia province, offshore sarawak, Malaysia. Mar. Petrol. Geol. 21, 517–534.
Zhang, B.M., Liu, J.J., 2009. Classification and characteristics of karst reservoirs in China and related theories (in Chinese with English abstract). Petrol. Explor. Dev. 36, 12–29. https://doi.org/10.1016/S1876-3804(09)60107-5.
Zhao, W., Shen, A., Quao, Z., Zheng, J., Wang, X., 2014. Carbonate karst reservoirs of the Tarim Basin, northwest China: types, features, origins, and implications for hydrocarbon exploration. Interpretation 2 (3), 65–90 (August 2014).